Part III

Prediction of Stress-Rupture Life of Glass/Epoxy Laminates in an Acidic Environment from Lamina Behavior

Abstract

A means to predict remaining strength and life of composite components in harsh environments and under complex time-varying loadings can help to optimize designs and cut costs. This paper reports an effort to predict the life of quasi-isotropic E-glass/913 epoxy composite laminates under constant load and in an acid environment. An experimental program involving stress-rupture tests of unidirectional coupons immersed in a weak hydrochloric acid solution was conducted to determine their stress-life response. Creep tests were conducted on unidirectional coupons parallel and transverse to the fibers, and on ±45° layups to characterize the lamina stress- and time-dependent compliances. These data were used in a composite stress-rupture life model, based on the critical element modeling philosophy of Reifsnider, to predict the life of two thickness-scaled quasi-isotropic laminates. Predictions compare favorably with experimental data.

Keywords: creep, stress-rupture, creep-rupture, stress relaxation, composite material, glass/epoxy, stress-corrosion cracking, durability, life.

1. Introduction

All-composite civil structures are appearing more frequently in load-bearing applications because of their low cost, light weight, and environmental resistance. Low cost glass-fiber/plastic composites are used in the process industry when the environment is highly aggressive and metal corrosion a serious problem. Some other applications are for storage tanks, piping, and in off-shore applications. These structures have tended to be overdesigned because material costs and reliability demands were low. As stresses rise and applications become more reliability sensitive (bridges for example), the need to design cost efficiently becomes even more important. For this reason, and because civil structures are asked to serve dependably for long periods of time, it is becoming increasingly urgent that engineers have tools to design composite structures for life, and not only for strength.

Creep of polymer composites, especially at elevated temperatures has been studied at length, and numerous models have appeared [1-4]. In comparison to fatigue, there is little work

on the time-dependent strength of composites under static loading. In part, this is because high performance applications of polymer matrix composites usually specify carbon fiber, which does not stress-rupture. Glass fibers are known to suffer stress-rupture behavior under static loading conditions when exposed to moisture, and other aggressive agents, especially acids. Some published results on stress-corrosion and stress-rupture of glass/polymer composites appear in references [5-19]. Very little exists in the literature on prediction of the stress-rupture life of composites in aggressive environments [20-22]. There is a need for characterization and modeling of the stress-rupture life of glass-fiber composite materials. A mechanistic modeling approach, called the critical element model, see Reifsnider and Stinchcomb [23], was developed for modeling fatigue life of composite materials. The framework of the modeling approach was used is this study to model the time dependent processes of creep and stress-rupture to predict life of composite laminates from the behavior of the laminae.

The experimental phase of this project was limited to six months duration. A composite material which could be environmentally conditioned so that it would exhibit stress-rupture type failures within the time constraint was needed. E-glass/913 epoxy was chosen because the E-glass fiber is known to be highly susceptible to stress-corrosion cracking when exposed to acids. Far superior fibers, such as R-glass, have been developed to resist stress-corrosion cracking due to acid attack. However, the stress-rupture life model could be tested as readily using either, and time constraints were severe.

In this Part, the experiments conducted to gather stress-rupture life data for unidirectional E-glass/913 epoxy lamina, and creep response parallel and transverse to the fibers, and in shear, is described. The stress-rupture life model used to predict the life of two ply-level scaled quasi-isotropic laminates under constant load is described. The purpose of examining ply-level scaled layups was to explore the possibility that under long term loading conditions, a size effect in the strength and stiffness might become more apparent via the nature of the damage developed. The results of the experiments on both the creep and stress-rupture tests are reported, and the failure modes are described. The predictions for creep and stress-rupture life are compared to the experimental data, and some possible refinements are noted. Comment is made on future work needed to expand the utility of the model to more general cases.

2. Experiments

2.1. MATERIALS AND SPECIMEN PREPARATION

The material used in this study was E-glass/913, a glass/epoxy composite supplied as unidirectional prepreg. Plates were made with in-plane dimensions of 300 x 300 mm and the following stacking sequences: $[0]_2$, $[0]_8$, $[90]_8$, $[+45/-45/+45/-45]_s$, and two ply-level scaled quasi-isotropic laminates $[0/90/+45/-45]_s$, and $[0_2/90_2/+45_2/-45_2]_s$. Laminates were cured as per the

manufacturers standard cure cycle at 120°C. All specimens, except for the 90's, were dry cut using a medium diamond wheel cut-off saw. The 90's were wet cut with a fine blade. The cut finish was not of a very high quality for the dry cut specimens. However, both edges of all specimens were wet ground on 240 grit silicon carbide paper until no visible defects remained. Grinding continued with 400 grit and finished with 600 grit paper to minimize the influence of any remaining microscopic defects. Specimens were found to be matrix microcrack free.

The creep/stress-rupture test frame with specimen installed is shown if Figure 1. Creep testing of composites having pinned end tabs requires special care in the surface preparation. The bond area of all specimens was grit blasted, then wiped with acetone. The aluminum end tabs were degreased and etched for improved bonding with the adhesive. The degreaser was a Minco 3410 aqueous alkaline degreasing bath, which was a non-silicate, non-caustic cleaner for aluminum. The chemical analysis was: Borax ($Na_2B_4O_7$) 38.0%, anhydrous Na_3PO_4 12.2%, extractable alcohol 9.6%, and deionized water 42.8%. This cleaner-concentrate was mixed with water at a ratio of 40 grams cleaner concentrate per one liter of water. The bath was circulated and its temperature kept at 60°C. The etch was a chromic/sulfuric acid pickle. The analysis for a 50 liter bath is: 3030 g chromic acid, 8600 ml sulfuric acid, 75 g aluminum, and 12 g of cupric-copper sulfate. The aluminum end tabs were suspended in the degreasing bath for 20 minutes, transferred into the first fresh water bath for 90 seconds, and then into the second fresh water bath for 20 minutes. The end tabs were transferred to the pickling bath and soaked for 30 minutes, then rinsed in fresh water baths for 90 seconds in one, and 20 minutes in the second.

Several types of aluminum end tabs were used. Quasi-static tensile test specimens had 50 x 25 x 1 mm thick aluminum end tabs. For the creep tests of $[90]_8$ and $[+45/-45/+45/-45]_s$ specimens, end tabs with 30° chamfer were used, see Figure 2(a,b). The stress-rupture test specimens had tabs with either a 4° or 30° chamfer. The 30° chamfer was intended for the more highly stresses specimens. All tabs with pin holes were closely machined so that the pin would have a very close fit. Stress-rupture specimens also required the clamp, as shown in Figure 2(a), to prevent debonding at higher loads.

All tabs were bonded to the specimens using a Redux 403 two-part epoxy paste adhesive. The rectangular tabs for the quasi-static tensile tests were aligned by eye, and pressure was applied using binder clips. The creep and stress-rupture tests needed precisely aligned tabs so that load would be evenly distributed between each tab, see Figure 2(b). The pin holes in the end tabs were aligned with a specially designed fixture. The specimen was aligned parallel and centered with the pin holes using guides in the same fixture. A uniform pressure was applied along the entire bond area of the tab, including the chamfered portion, by using a spring loaded bar having matching chamfers. The adhesive bond was allowed to cure overnight at room temperature, then specimens were placed in an oven at 60°C for at least one hour.

2.2. QUASI-STATIC TENSILE TESTING

Quasi-static tensile tests were conducted using a Zwick 100 kN capacity screw driven universal test machine. The grips were of the wedge action type. Strain was recorded using a clip-on extensometer having a 20 mm gauge length, and able to average out-of-plane bending. Load and strain were recorded on an x-y chart recorder. The crosshead speed was 2 mm/min. Specimens were loaded until the strain reached about 1%, then the extensometer was removed, and loading continued until failure. The stress at the onset of matrix cracking was also recorded.

2.3. CREEP AND STRESS-RUPTURE TESTING

2.3.1. *Strain Measurement*

Strain was recorded for both creep and stress-rupture tests using a pair of extensometers having capacitive type transducers. Readings were averaged, unless one became clearly incorrect. A photograph of a specimen ready for a creep test was given in Figure 1. The reliability of the transducers was verified by measuring the elastic modulus and comparing the readings to those obtained from the clip gage used in the quasi-static tensile tests. Readings were in agreement.

2.3.2. *Environmental Conditioning*

The temperature and humidity of the environment in which the stress-rupture tests were performed was precisely controlled. All specimens were kept in the open air of the lab until ready for testing. No specimen was tested until after having been stabilized for at least four months. Therefore, it was assured that the moisture content of all the specimens was uniform and at equilibrium when the tests were initiated. In the case of the 90° and ±45° angle-ply specimens the moisture content remained stable for the duration of the test.

The laminates were immersed in tap water at 60°C for one week, then were dried in an oven at 60°C for an additional week. This treatment is known to reduce the fracture toughness of the matrix. All specimens were subjected to this treatment, except the 2-ply unidirectional ones.

A stress-corrosion cracking environment was simulated by submerging opposing faces of the specimen (exclusive of edges) in a dilute (0.01 molar) hydrochloric acid solution. A photograph of the specimen with environment chambers attached is shown in Figure 3. Thin glass slides, 37 x 25 mm, were bonded on three edges to the gage section of the specimen using a clear silicon rubber sealant. Spacers were used to create a 2 mm wide gap between the specimen and the glass. The edges of the specimen were sealed to prevent the environment from penetrating by interfacial diffusion or by following a void or crack. Diffusion could only occur through the matrix into the front and back faces of the specimen. The region of the specimen below the chambers was wrapped in an absorbent tissue to soak up acid in case fracture of the specimen also

breached the chamber. Just before the tensile load was applied to the specimen, the chambers were filled with the acid by inserting a pipette through a small opening in the bag. To protect personnel and equipment from acid that might splash during rupture of the specimen, the entire gauge section was jacketed in clear plastic, and openings were sealed with a tacky adhesive cord normally used as a vacuum bag sealant, as shown in Figure 2(a).

2.3.3. Creep Tests

Loads were selected for the creep tests of the 90° and ±45° angle-ply specimens to induce strains similar to that which was experienced by the quasi-isotropic laminate. The 90° specimens were loaded at stresses ranging from 15 to 35 MPa. The ±45° specimens were loaded at stresses ranging from 30 to 100 MPa (this was axial stress on the coupon, not shear stress). Creep data was also obtained for the unidirectional specimens, with loads chosen based on expected life.

2.3.4. Stress-Rupture Tests

Stress-rupture tests were carried out on the 2-ply unidirectional, and the 8-ply and 16-ply quasi-isotropic specimens. Strain and time to failure were recorded. Failure was defined as complete separation of the specimen. The loads were selected, by trial and error, so that failures occurred in the range between 10 and 1700 hours.

3. Stress-Rupture Life Modeling

The stress-rupture life of the two quasi-isotropic laminates is modeled using the microkinetic approach developed by Reifsnider [23-25]. These are good recent references to introduce the reader to this modeling philosophy, and a variety of different cases are examined there. The most accurate and reliable predictions of the residual strength (damage tolerance) and life (durability) of a composite require careful laboratory observations of actual damage modes exhibited by the specific material of interest. How the various material properties change over time, including the stiffnesses and strengths, and the time and sequence of their appearance need be known. These properties can be quantified with time- and stress-dependent functions that represent strengths and compliances. The compliances can be fed to a classical laminated plate analysis module to get time-dependent stress in the critical element. In the case examined here, the critical element is represented by 0° plies because their failure induces total failure of the laminate. The experimental work needed to describe the change in the stress state in the 0° plies of the laminate are described in the section on experiments. The change in the various compliances with time and stress was characterized from viscoelastic creep tests.

The "life integral" is described next, but only in relation to how it is used here. The stress-rupture life model incorporates experimentally-obtained applied stress versus life response, and viscoelastic creep-compliance responses of the laminae.

3.1. ESTIMATION OF REMAINING STRENGTH AND LIFE

From the microkinetic theory, there is an equation that relates changes in the state of stress in the critical element, and changes in the material state of the critical element, as a function of the global loading history, to remaining strength and life of the material. The critical element of a composite laminate is identified as that part of a representative volume that defines failure, meaning that its failure signals global component failure. For a composite coupon, the critical element is identified as being those plies whose failure (in this case) signals complete failure of the laminate. For structural laminates, the critical element is usually taken to be the primary load bearing plies; here they would be the 0° plies oriented with the tensile loading. The strength and stiffnesses of the critical element define its material state, and may be affected by time, temperature, cyclic mechanical and/or thermal loading, and environmental degradation. This study was concerned with how the durability (life) of the critical element (the 0° plies) was affected by time-varying tensile stress when exposed to hydrochloric acid, an aggressive agent known to seriously degrade the strength of E-glass fibers. The strength and life of the critical element is influenced by subcritical elements.

Subcritical elements constitute the portion of the representative volume, which may undergo change, but the changes do not signal global component failure. The changes most often considered are those which cause stress redistributions in the critical element. Some examples are matrix microcracking, aging, stress relaxation, and delaminations, each of which degrades component stiffness, and increase (usually, but not always) the stress on the critical element. The experimental portion of this study was designed so that only stress redistribution (due to stress relaxation in the various plies) would affect the stress in the critical element. The laminate was designed to not delaminate, and matrix cracking (especially in the 90° plies) was avoided by conducting the tests at loads below the first-ply failure stress.

The total cycles to failure, N (time, in this case), is modeled after the stress-rupture life of the 0° plies and is taken to be

$$N = 10\wedge\left\{\left[\frac{\frac{\sigma_{11}}{X_t} - A}{B}\right]^{1/p}\right\} \tag{1}$$

where X_t is the instantaneous tensile strength of the 0° plies, σ_{11} is the fiber-aligned stress in the 0° plies, and A, B, and p are experimentally determined coeffcients. The remaining strength, F_r, starts at 1, and is given as

$$F_r = 1 - \int_0^{n/N} (1 - F_a) j \left(\frac{n}{N}\right)^{j-1} d\left(\frac{n}{N}\right) \tag{2}$$

and depends upon the elapsed time, *n*, and the projected time to failure, *N*. The expression for F_a is

$$F_a = \frac{S_a}{S_u} = A + B(\log N)^p \tag{3}$$

and is defined as the applied stress in the critical element, S_a (σ_{11} before), divided by the ultimate strength of the critical element, S_u (X_t before). The coefficients A, B, and p are experimentally determined from a series of stress-rupture tests of unidirectional coupons at different stresses.

The coefficient, *j*, affects the shape of the remaining strength curve. Depending upon its value, the strength can appear to drop off gradually over time, or drop suddenly at the end (called sudden death). When *j* is low, strength is modeled as dropping gradually during most of the life, accelerating near the end. When *j* is high the strength is modeled as undiminished for much of the life, and dropping very rapidly at the end. Direct remaining strength data were not taken for this work, so a correct value for *j* is not known, but was thought to be high, therefore a value of 7 was chosen. In this study, there was no significant effect of the value of *j* on the remaining life predictions because the applied stress changed little during the test. The ultimate strength of the critical element, S_u, can be dependent on time and temperature. In this model, the strength of the glass fibers is degraded over time under the action of the acid environment. The applied stress on the critical element, S_a, is also time dependent because the compliance of the subcritical elements vary with time and stress.

3.2. MODELING LOSS OF STRENGTH IN THE UNIDIRECTIONAL PLIES

The stress-rupture process of E-glass/913 epoxy composite is well described by Hogg [9], and Hogg and Hull [10]. The acid diffuses through the polymer matrix until it reaches the fibers. Then a chemical reaction occurs which weakens the fibers so that, when under tension, a very clean crack propagates. Once a crack has started through the fibers, the matrix may also crack. If so, acid is rapidly transported to the surfaces of the unbroken fibers. Diffusion of acid through the matrix then becomes a second order transport process, as acid is directly introduced to the surface of intact fibers. Cracks can then grow more quickly and so the remaining strength falls more

quickly. Cracking also accelerates because the decreasing cross section raises the mean stress on the intact fibers. The crack growth process in individual fibers, or in the lamina was not modeled. Instead, the life of the critical element as a function of time and stress was determined by fitting a curve to a series of stress-rupture tests conducted at various tensile loads. Equation 1 was rearranged as Equation 3 for this purpose, and the coefficients, A, B, and p are selected for a best fit.

3.3. CREEP MODEL OF COMPLIANCE CHANGE

The change of the transverse and shear moduli as a function of stress and time are incorporated into the life predictions because these changing compliances change the stress in the critical element. Laboratory creep data was taken parallel to the fiber direction using the $[0]_2$ specimens, transverse to the fiber direction using the $[90]_8$ specimens, and in shear by use of the $[+45/-45/+45/-45]_s$ tensile specimens. The compliances, S_{ij}, were obtained from the strain data, ε_{ij}, using the relations:

$$S_{11}(t)= \varepsilon_{11}(t)/\sigma_{11},\ S_{22}(t)=\varepsilon_{22}(t)/\sigma_{22},\ \text{and}\ S_{66}(t)=\gamma_{12}(t)/\tau_{12},\ \text{where}$$

$$\gamma_{12}(t)= \varepsilon_{xx}(t)(1+\nu_{\pm 45})\ \text{and}\ \tau_{12}=\sigma_{xx}/2. \tag{4}$$

The symbols σ_{11}, σ_{22}, τ_{12}, are lamina-coordinate principal stresses. The time-dependent shear strain is $\gamma_{12}(t)$, and the formula for it is from Rosen [27]. Poisson's ratio of the ±45's is symbolized by $\nu_{\pm 45}$, and was assumed to remain constant. The fiber direction time-dependent compliance, $S_{11}(t)$, was represented using the linearized Findley [4] fitting function:

$$S_{11}(t)=S_{11}(0)+At^n, \tag{5}$$

where the coefficient $S_{11}(0)$ is the initial elastic compliance, while A and n are coefficients used to fit the experimental data.

The transverse time-dependent compliance, $S_{22}(t)$, was also represented using the linearized Findley fitting function:

$$S_{22}(t)=S_{22}(0)+At^n, \tag{6}$$

where the coefficient $S_{22}(0)$ is the initial elastic compliance, and A and n are a second set of coefficients used to fit the experimental data.

The shear compliance, $S_{66}(\tau_{12},t)$, was represented using Lou and Schapery's [3] quadratic fitting function:

$$S_{66}(\tau_{12},t) = S_{66}(\tau_{12},0)\left[1+g\tau_{12}^2\right]+m\left[1+f\tau_{12}^2\right]t^n \tag{7}$$

where the coefficient $S_{66}(0)$ is the initial elastic shear compliance at a computed shear stress τ_{12}, and *g, m, f,* and *n* are coefficients used to fit the experimental data accounting for both stress and time. The FORTRAN computer code written for this problem is given in the Appendix. The classical laminated plate theory portion used in the stress analysis is omitted there.

3.4. OTHER MECHANISMS INFLUENCING LIFE

There are a host of other material changes and damage forms which can significantly influence life. Two that act on life in this study are mentioned now, others are relegated to the future work section. Matrix cracking in off-axis plies cause stress concentration in neighboring plies. This stress concentration and the overall stiffness change could be represented using a simple shear lag model [26]. Cracks also could provide a path for transport of the acid bath. In this study, matrix cracking did not appear at any time during the life, at least not until 0° stress corrosion cracks appeared. The justifications for ignoring their effects are discussed in Section 5.3.4.

4. Results

4.1. QUASI-STATIC STRENGTH TESTS AND DAMAGE CHARACTERIZATION

4.1.1. Unidirectional $[0]_8$ Specimens

The moduli and strengths are given in Table 1. The post-failure morphology has a broom-like appearance, Figure 4(a). Closer inspection suggests that cracks can grow across the fibers for some characteristic distance before a split begins and stops the crack from breaking more fibers. The first fibers to fracture were at the edge, and very near the grip. A progression of fiber bundle fractures and splitting progressed across the width of the specimen. The fiber bundles were approximately 1.5 to 2.5 mm wide, and from one to eight plies thick. For the moment, I presume that the length of the crack that ran across the fibers is dictated by the magnitude of the shear and peel stresses that can be supported before a split forms and runs along the length. After the first fibers fracture and a bundle splits, all subsequent fiber fracturing occurred at either grip. This sequence repeated itself until each half of the failed specimen looked broom-like and about the length of the gauge section.

4.1.2. Quasi-Isotropic Specimens

8-ply Quasi-Isotropic $[0/90/+45/-45]_s$ specimens Matrix microcracking in the 90° plies occured before the ultimate tensile load was reached. A failed tensile test specimen is shown in

Figure 4(b). Both specimens tested, Q8-6 and Q8-8, exhibited a very straight fracture across the surface 0° ply on one side which extended for 2.6 and 2.9 mm, respectively. Failure initiation was well away from the grip. Then, short splits begin to appear in the 0° ply which was accompanied by growing randomness in the location for continuation of fracturing of the fibers. The length of the splits was at first very small, about 0.5 mm or less, but became longer as the fracture progressed across the specimen width. The width of the splits was less than a millimeter. As the 0° ply fractured, the +45° ply developed damage in the form of microcracks, reducing the constraint with the 0/90 sublaminate, which then delaminated. There were no fiber failures in 45° plies. The length of the fracture zone was 30 and 36 mm, and was defined by the region of shear out of the 45° plies.

16-ply Quasi-Isotropic $[0_2/90_2/+45_2/-45_2]_s$ specimens Failure of Q16-5 was at the grip, and Q16-3 failed one specimen width away from the grip, and is shown in Figure 4(c). Both became saturated with 90° cracks, but there were also -45° cracks and perhaps some +45° cracks. Failure of the surface 0° plies started on one side of the specimen at the edge and progressed across the width. During this period load sheds to the underlying 45's which quickly strain, crack, and shed most of the load onto the 0° plies on the opposite face. Some fracturing of the 0° fibers occurred near the original crack, but very quickly long splits blunted them, and the remainder of the 0° plies failed in the manner of the unidirectional specimens. About half way across the width, the splitting became completely unrestrained and ran along the length of the specimen. This splitting behavior was observed in the unidirectional specimens.

4.2. VISCOELASTIC CREEP TESTS

4.2.1. Lamina Creep Characterization

Creep tests of $[0]_2$, $[90]_8$, $[+45/-45/+45/-45]_s$ specimens were conducted at room temperature (21°C) to characterize the time-dependent and stress-dependent compliances. The initial elastic compliances, $S_{22}(0)$, and $S_{66}(0)$, were measured using the extensometers and appear in Table 2, but these data were not tight.

The strain-time plots for the unidirectional tests are shown in Figures 5, 6, and 7. These creep plots share the same features as observed in metal creep. There are clearly defined primary, secondary, and tertiary creep phases. At the scale shown in these figures, the primary creep is difficult to see, but is there, and will be examined more closely. The secondary creep phase dominated the life of the unidirectional specimens. Tertiary creep represented the final phase in the life, and was due to the nucleation and growth of stress-corrosion cracks. Observations about the stress-corrosion cracks are made in Section 4.3. A significant simplifying assumption made was that the unidirectional specimens could be represented as having failed catastrophically. The presence of a tertiary creep phase made this assumption invalid in a strict sense. However, from

inspection of Figures 5, and 6, it was judged that the fraction of the life which was composed of tertiary creep was small and could be neglected. Unidirectional creep data were converted to compliance data and are shown in Figure 8. All the data was plotted together. A single Findley curve representing $S_{11}(t)$ was fit to the data. The fitting coefficients used in Equation 5 were:

$$S_{11}(0)=2.07\text{x}10^{-11},\ A=2.97\text{x}10^{-13},\ \text{and}\ n=0.200$$

Only one curve was needed because there did not appear to be any dependence of compliance on stress, only on time. The curve fitting function chosen did not include tertiary creep because it was argued that failure could be regarded as catastropic. In Figure 9, the time scale of Figure 8 is expanded to include only the first 10^6 seconds. The purpose was to show that, aside from tertiary creep, the chosen fitting function represented fairly well the primary and secondary creep phases.

Creep testing of the 90° and the ±45° specimens was conducted in a controlled temperature, controlled humidity environment. All the creep data for the 90's was converted to compliance, $S_{22}(t)$, data and was plotted together in Figure 10. There was no observed stress dependence, at least for the range of stresses considered, nor was there a tertiary creep phase either. Hence, compliance could be represented by a single Findley fitting function. The form of the function was given in Equation 6, and the values for the coefficients used to fit the data are:

$$S_{22}(0)=5.62\text{x}10^{-11},\ A=3.629\text{x}10^{-13},\ \text{and}\ n=0.355$$

The shear compliance, $S_{66}(\tau_{12},t)$, was observed to be dependent on both the applied stress, τ_{12}, and time, t. The data and corresponding curve fits appear plotted together in Figure 11. Lou and Schapery's quadratic fitting function (Equation 7) was used. The coefficients used to fit the data are:

$$S_{66}(0)=1.1\text{x}10^{-10},\ g=2.8\text{x}10^{-16},\ m=12.36\text{x}10^{-15},\ f=1.0\text{x}10^{-13},\ \text{and}\ n=0.37$$

4.2.2. Quasi-Isotropic Creep Data and Predictions

Creep data were taken during all stress-rupture tests of the 8-ply quasi-isotropic specimens, shown in Figures 12, 13, and 14, and for 16-ply quasi-isotropic specimens, shown in Figures 15, 16, and 17. By use of the forgoing compliance-time responses of the lamina, it was possible to make predictions of the creep response of the quasi-isotropic layup. Creep tests are compared with the predicted creep response for three different loadings, and consequently, three different lives, see Figure 18. A short life test of a 16-ply quasi-isotropic specimen at 154 MPa is shown in Figure 18(a). The prediction tracks the data closely; only during the tertiary phase, where stress-corrosion cracking is ongoing, is deviation significant. In Figure 18(b), the intermediate life test is of an 8-ply quasi at 112 MPa. Again, agreement is quite good.

Not until long life creep tests were modeled did a clear error appear. A long life test of an 8-ply quasi at 80 MPa is shown in Figure 18(c). Underprediction of creep at long times suggests that moisture absorption may be causing both moisture expansion and an increase in compliance.

4.3. STRESS-RUPTURE TESTS AND DAMAGE DEVELOPMENTS

Stress-Rupture testing was performed on $[0]_2$, $[0/90/+45/-45]_s$, and $[0_2/90_2/+45_2/-45_2]_s$ specimens in the presence of dilute (0.01 molar) hydrochloric acid.

4.3.1. Stress-Rupture of Unidirectional $[0]_2$ Specimens

Eight stress-rupture tests of unidirectional $[0]_2$ specimens were performed. In each case the strain vs. time response was typical of that of an ordinary creep test, see Figures 5, 6, and 7. No indication of the chemical processes being undergone within the fibers was apparent because no interrupted strength tests were performed. Therefore, how the strength might vary before the appearance of stress-corrosion cracks was unknown. Stress-corrosion cracks were observed to grow to lengths dependent upon the tensile load on the specimen. The number of stress-corrosion crack nucleation sites was greatest for the highest applied tensile stress test. The length that a stress-corrosion crack grew before a split formed depended upon the applied tensile stress; lower stresses permitted longer cracks to grow. The splits effectively reduced the cross section of the specimen, and raised the total strain in the remaining material. For the higher stressed specimen (225 MPa), in Figure 19, most of the individual stress-corrosion cracks are less than 1 mm in length. Also, a large number of cracks form. This explains the tortuous fracture profile. For the case of the lower stressed specimen (185 MPa), in Figure 20, there were two long cracks: one 9 mm, and one 3 mm long. The remaining cross-section became highly stressed, and a large number of small cracks formed, accompanied by extensive splitting. The basic process then, was to form few long cracks which grew normal to the applied load, then to transition to a combination of large numbers of short cracks with splitting, as the effective stress increased. Cracks typically grew completely through the thickness of these two-ply specimens. Some high stress tests (tensile loads of approximately 70% of quasi-static strength) were conducted in high strength acid baths (1 molar HCl) on 8-ply specimens. In those cases, cracking was usually arrested by delamination of the surface-cracked ply, and by splitting.

All stress-rupture life data was plotted as normalized applied stress to ultimate strength (S_a/S_u) vs. time to failure in Figure 21. Then a curve was fit to the data using the function indicated in Equation 3, resulting in values for the coefficients of A=1, B=-0.294, and p=0.582. Short duration life data of less than 10,000 seconds was lacking. In order to help the curve fitting routine to correctly traverse the gap, data from a single $[0]_8$ stress-rupture test was inserted into the plot. There were two inconsistencies in doing so. The specimen was four times thicker, and the acid concentration was 10 times sronger. The two inconsistencies cancel each other to some extent, so

it was judged that the error was not severe, and would outweigh the problem of omission. Without the short-life data point, the curve fitting routine would give an extremely rapid drop in normalized applied stress for a small increase in life, which was not realistic.

Three of the long-life tests were interrupted before failure (as indicated by the arrows). As a consequence, the fit curve has a built in lower bound on the low-stress/long-life portion of the curve.

4.3.2. Stress-Rupture of Quasi-Isotropic Specimens

Strain - Time Plots The strain vs. time plots are a rough indicator of the onset of damage, because as the cracks nucleate and grow the strain in the gage section increases rapidly. Strain vs. time plots for each quasi-isotropic stress-rupture test was given beginning with Figure 12 and continuing through to Figure 17. Except for the short duration tests of the 8-ply quasi's in Figure 12, it can generally be observed that the strain vs. time response is mainly that of ordinary creep, with a brief tertiary phase indicating the nucleation and rapid propagation of cracks.

Stress-Corrosion Crack Nucleation and Initiation of 90° Cracks Generally, the higher the far field stress, the larger the number of stress corrosion cracks that nucleated. The preferred location of the fracture line was close to the meniscus, or just below it, although perhaps a quarter of failures were well below the meniscus. Matrix cracks parallel to the fibers in the 90° plies would have the effect of concentrating stress in the unidirectional plies (the critical element) and so it was needed to verify whether or not these cracks appeared at any time during the test. From the quasi-static tensile tests, it was known that matrix microcracking starts at 215 MPa for the 16-ply. For the 8-ply, matrix microcracking was not heard at any time until the failure stress of about 320 MPa. Therefore, 90° matrix cracks were not anticipated because stress-rupture tests for 8-ply quasi's were conducted at stresses not more than 1/3 of the cracking onset stress (1/2 for 16-ply quasi's). To determine whether cracks appeared at any time, the failed specimens were first examined for the appearance of matrix cracks outside the region exposed to the environment. None were found. For the region within the environment, the presence of 90° matrix cracks without an accompanying 0° stress-corrsion crack was searched for, but none were found. Finally, when 0° stress-corrosion cracks existed, there were also 90° matrix cracks underlying them.

The evidence supports formation of 90° cracks after the nucleation of a 0° stress-corrosion crack. An advanced stress-corrosion crack, with a 90° crack which extended for the entire width, appears in the photo of the fractured specimen in Figure 22. A schematic drawing is given in Figure 23. It was clear that once a 0° stress-corrosion crack had nucleated and propagated through the thickness of the ply, then, a crack in the adjacent 90° ply initiated. The 90° cracks grow well

ahead of the 0° cracks. This likely guides growth of the 0° crack due to both the local stress concentration, and ingress of environment to the interior of the laminate. From the 0° tests it was already known that the cracks prefer to propagate normal to the applied load, at least until the stress was high enough to start a split. The presence of the off-axis plies supressed splitting, which further encouraged the cracks to remain in a line.

Stress-Corrosion Cracking of the ±45° Plies Inspection of completely failed specimens reveals that stress corrosion cracking forms in the +45° plies adjacent to the 90° crack, and in some cases also penetrated the middle -45 ° plies, see Figures 24 and 25. This scenario was more prevalent for the lightly loaded specimens. The more highly stressed specimens were less likely to have stress corrosion in the 45's, see Figure 22. There was simply less time for stress corrosion cracking to either initiate or progress very far into the 45° plies before the 0° plies could no longer support load.

Appearance of the Fracture Profiles The final failures look slightly different between the 8-ply (Figure 24), and 16-ply (Figure 25) specimens. The very region which looked different is the portion of specimen with the remaining ligament of 0° plies. This part failed due to tensile overload, and looks much like the fracture morphology as was described in Section 4.1.2.

4.4. STRESS-RUPTURE LIFE PREDICTIONS

Predictions of stress-rupture life of the 8-ply quasi-isotropic specimens under a steady tensile load and immersed in 0.01 molar HCl acid is given in Figure 26, and for 16-ply quasi's in Figure 27. The predicted life locus (solid line) runs between the data points. For the 8-ply, prediction appears slightly high, while the prediction for the 16-ply is almost perfect. The dashed line is the predicted life locus if creep in the off-axis plies is ignored, and shows that overprediction of life results. The error amounts to roughly a factor of two increase in the life prediction.

5. Discussion

5.1. QUASI-STATIC TENSILE STRENGTH DATA

5.1.1. Unidirectional $[0]_8$ Tensile Tests

All failures of unidirectional $[0]_8$ specimens were close to the grip, indicating the predominance of grip region stress concentration. Correct strengths are obviously preferable, so a correction factor was sought. Work done by O'Brien *et al.* [28] gives finite element analyses of grip region stress concentration. They compute a stress concentration of nearly 1.2 for the graphite/epoxy material they modeled. The degree of orthotropy (E_{11}/E_{22}) was shown to affect the

stress concentration. Since the unidirectional glass/epoxy had an orthotropy ratio of 3.3 (11.6 for the unidirectional carbon/epoxy), it was accepted that the correction factor of 1.2 was not strictly correct. The strength actually used in the predictions was raised by a factor of 1.2 from 862 MPa to 1034 MPa. Having established that initiation of the fiber fracturing near or at the grip should be expected, the issue of the splitting is addressed. For organic matrix composites, the poor interfiber fracture toughness makes it likely that cracks running across fibers will reorient themselves toward the direction requiring the least energy to continue the fracture. Unidirectional composite, lacking constraint against splitting, will prefer to split, as was seen in Figure 4(a). The effect of ply constraint on resistance to splitting was addressed by Stinchcomb, Reifsnider, Yeng, and Masters [29].

5.1.2. Quasi-Isotropic Specimens

There was no splitting of the surface unidirectional plies outside of the damaged zone in the 8-ply quasi-isotropic specimens, but there was for the 16-ply specimens. The unrestrained splitting behavior seems to occur depending upon the thickness of the 0° plies. Stress redistribution around a stress-corrosion crack drives peeling and splitting of the bundle of fibers from the laminate, and this depends on thickness. It would appear that to control unrestrained splitting of surface zero degree plies, their thickness must not exceed some threshold that can probably be related to the stiffnesses and interfiber fracture toughness.

5.2. CREEP TEST DATA

A thorough calibration of the extensometers (to meet ISO 9001 standards) was performed late in the experimental program. Though the transducers passed, this did not assure smooth creep data. The extensometers were designed for shorter, stiffer specimens than used here. It was especially difficult to obtain smooth creep data from the 2-ply 0° and 8-ply 90° specimens, because of their flexibility.

The setup for each test was long, and often needed to be repeated until good elastic modulus measurements were obtained. Correct elastic modulus data was a good indicator that the extensometers were installed well, but was no guarantee that data would continue to be smooth. Good results often depended on talent, experience, or just luck. This suggested that although ISO 9001 standards were met when the extensometers were mounted on a calibration rig, it did not mean they will be met when mounted to a composite test specimen. Further work should be done to establish the allowable bending stiffness of composite creep specimens to ensure smooth creep data when using these extensometers.

5.2.1. Unidirectional $[0]_2$ Creep Tests

The measured creep response of the unidirectional specimens was actually a combination of creep and the influence of moisture expansion due to moisture uptake during the stress-rupture tests. Tests were not conducted to characterize moisture absorption effects independently from the creep response, therefor the relative contribution of each to the compliance change was not known. However, as both the unidirectional and quasi-isotropic tests were under the same temperature and moisture conditions, the compliance data of the unidirectional specimens should accurately represent the changing compliance of the same plies in the quasi-isotropic specimens.

5.2.2. Fitting Curves to the $[+45/-45/+45/-45]_s$ Creep Tests

The curve fit for the shear compliance, $S_{66}(\tau_{12},t)$ is not as good as for $S_{11}(t)$ or $S_{22}(t)$, as is clear when Figures 8 and 10 are compared to Figure 11. Choosing the coefficients was actually a lengthy trial and error process because the curve fitting software used could not simultaneously optimize the fit to all curves. Rather, a fit was found for one curve and then the coefficients were adjusted until all other curves were approximately represented. The coefficients were chosen so that the predicted responses fell within the bounds of the experimental data.

The initial elastic shear modulus from extensometer data was taken while loading the pan of the creep frame, and appears in Table 2. The data is highly scattered. Apparently the relative slowness of loading the pan allowed the large initial viscoelastic response to literally creep into the elastic measurements.

5.2.3. Moisture Absorption Effects on Creep Response and Life

Moisture absorption influenced the overall creep response of the quasi-isotropic specimens at long test times, as was shown in Figure 18(c). The computed stress on the critical element should be correct if the creep response can be correctly predicted, at least before any cracks formed. Since creep in the long time tests is actually greater than predicted, the computed stress in the critical element will be low, and the life over-predicted.

Only the viscoelastic creep at room temperature of dry specimens was measured to form representations for $S_{22}(t)$ and $S_{66}(\tau_{12},t)$. To account for the effects of moisture requires additional tests. One test is to characterize the rate of diffusion of the HCl acid bath into the laminate. Another test is to obtain the moisture expansion coefficients. Finally, additional creep tests to characterize the dependence of compliance on the moisture content are needed.

5.3. STRESS-RUPTURE LIFE

5.3.1. Experimental Variability

Experimental variability in the stress-rupture life data was observed (see Table 3, and Figures 26 and 27). Of three tests at the same stress level, two would often have virtually identical lives, and the third would be an outlier. No scratches were found on any specimens that might be blamed for early exposure of the fibers to the acid. Nor was there any correlation between life and specimen thickness. The rationale for a correlation between the two is that fiber volume fraction, V_f, and thickness are often strongly correlated. Stresses calculated from cross-sectional area will not necessarily be related to stress on the fibers unless V_f is known. Furthermore, a high V_f means less resin to protect the fibers from the acidic environment. This said, there were too few tests at any one stress to find a correlation between life and thickness.

5.3.2. Model Predictions

Applied stress versus stress-rupture life plots of experimental data for the 8-ply $[0/90/+45/-45]_s$ specimens and for the 16- ply $[0_2/90_2/+45_2/-45_2]_s$ specimens was given, along with a predicted life locus, in Figures 26 and 27, respectively. At first glance, the predictions look good for both 8-ply and 16-ply specimens. The apparent success of the predictions rests upon two observations. First, relative to the total life of the specimen, failure occured shortly after the first stress corrosion cracks appeared. Second, the positioning of the 0° plies on the outside of the laminate simplified the problem by eliminating the need to consider the rate of diffusion of the environment through protective plies.

All the creep was not accounted for, especially at long times, as was shown in Figure 18(c). The additional creep was likely due to moisture uptake. Life predictions would be expected to be high, which seems to be the case. Creep significantly affects life, but is less than an order of magnitude effect, at least at room temperature. At elevated temperature creep will play a much more significant role. Diffusion rate and corrosion rate would also be significantly affected by temperature [20]. Characterizing temperature effects on rates of creep, corrosion, and moisture diffusion will be important to predicting life of more complex loading cases and more challenging laminate stacking sequences.

5.3.3. Effect of "n" on Stress-Rupture Life of $[0]_n$ Unidirectional Specimens

The thickness of the quasi-isotropic specimens affects their life when exposed to the HCl acid. The thicker specimens last longer. To model the effect of thickness on life of the unidirectional laminates was beyond the scope of this study. In order to eliminate this variable, the original seventeen 8-ply unidirectional specimens were replaced with a new set of ten 2-ply

specimens. This was the reason for the sparsity of data available to define the stress vs. life response.

5.3.4. *Other Damages to the Sub-Critical Elements: Observed, Yet Unaccounted For*

Matrix Microcracking If the 90° plies in the quasi-isotropic laminate had cracked at any time during the stress-rupture test, then the stress concentration on the 0° plies would need to be included. From both quasi-static tensile tests and stress-rupture tests of the quasi-isotropic specimens it was known that the threshold stress at which cracks initiated in the 90° plies was well above the stresses used in the stress-rupture tests. Matrix microcracking was only observed to form in the 90° plies once cracking in the 0° plies had begun. However, as this occurred very late in the life of the specimen it was judged not to be a significant factor influencing the total life.

Stress-Corrosion Cracking It is expected that once a 90° crack forms (as was observed in response to formation of 0° cracks, as was shown in Figures 22 and 23), that the environment would be transported along the crack and into the laminate where interior plies would come under attack. These events did occur, as was clear from Figures 24 and 25. Substantial portions of the 45° plies were cracked. It was assumed that the additional life would be brief once 0° cracks appeared, and so stress-corrosion cracking of off-axis plies was ignored, as was the resulting increased stress on the critical element.

5.4 FUTURE WORK

Considerable further work is needed to model stress-rupture life of more general problems. The laminate studied here was deliberately chosen to avoid delamination and a host of other anticipated complications. What follows is a list of complicating effects, more general loadings, and environmental conditions which should be examined in the laboratory and incorporated into the model.

1) Characterize the effects of moisture on expansion and compliance, and hence on life.

2) High stress testing should be conducted on laminates made with acid resistant glass fibers, such as R-glass. Then, the effect of matrix microcracks neighboring to load bearing plies on long term life due to stress concentration and/or the crack serving as a path for rapid ingress of acid can be studied. This information can be used to model the way load bearing, but subcritical elements crack and shed load to the critical element.

3) Effect of temperature on the rate of diffusion of the environment to both surface and subsurface load bearing plies.

4) Incorporate effects of fatigue and transient overloads [16]. This will necessitate well characterization of the remaining strength will time and stress.

5) Investigate the potential to use short term elevated temperature tests to predict long term life.

6. Conclusions

Stress-rupture life of E-glass/913 quasi-isotropic composite laminates has been predicted from lamina stress-rupture life data, and creep response, using a mechanistic stress-rupture life model based on the critical element modeling philosophy. The effects of creep in the various plies has been shown to significantly affect the prediction of stress-rupture life. Increasing thickness by ply-level scaling was found to increase the life because there was more material to be degraded.

7. References

1. Sturgeon, J.B. (1978). Creep of Fibre Reinforced Thermosetting Resins. in Creep of Engineering Materials, A Journal of Strain Analysis Monograph, edited by C.D. Pomeroy, Mechanical Engineering Publications Limited, London, Chapter 10, pp. 175-195.

2. Scott, W.D., Lai, J.S., and Zureick, A.-H. (1995). Creep Behavior of Fiber-Reinforced Polymeric Composites: A Review of the Technical Literature. Journal of Reinforced Plastics and Composites, Vol. 14, June, pp. 588-617.

3. Lou, Y.C., and Schapery, R.A. (1971). Viscoelastic Characterization of a Nonlinear Fiber-Reinforced Plastic. Journal of Composite Materials, Vol. 5, pp. 208-234.

4. Findley, W.N., Lai, J.S., and Onaran, K. (1976). Creep and Relaxation of Nonlinear Viscoelastic Materials. New York: Dover Publications.

5. Heywood, R.B. (1961). The Fatigue and Stress-Rupture Properties of Some Glass Reinforced Polyester Laminates. Royal Aerospace Establishment Tech Note Chem 1376, February.

6. Steele, D. (1965). The Creep and Stress-Rupture of Reinforced Plastics. Trans. J. Plastics Inst., Vol. 33, pp. 161-167.

7. Lyons, K.B., and Phillips, M.G. (1981). Creep-Rupture and Damage Mechanisms in Glass-Reinforced Plastics. Composites, October, pp. 265-271.

8. Aveston, J, and Sillwood, J.M. (1982). Longterm Strength of Glass Fibre Reinforced Plastics in Dilute Sulphuric Acid. Journal of Materials Science, Vol. 17, pp. 3491-3498.

9. Hogg, P.J. (1983). Factors Affecting the Stress Corrosion of GRP in Acid Environments. Composites, Vol. 14, No. 3, pp. 254-261.

10. Hogg, P.J., and Hull, D. (1989). Progress in Rubber and Plastic Technology, Vol. 5, pp. 112-155.

11. Jones, F.R., Rock, J.W., and Bailey, J.E. (1983). The Environmental Stress Corrosion Cracking of Glass Fibre-Reinforced Laminates and Single E-glass Filaments. J. of Materials Science, Vol. 18, pp. 1059-1071.

12. Jones, C.J., Dickson, R.F., Adam, T., Reiter, H., and Harris, B. (1984). The Environmental Fatigue Behaviour of Reinforced Plastics. Proceedings of the Royal Society of London, A 396, pp. 315-338.

13. Jones, F.R., and Rock, J.W. (1984). A Method for Determining Crack Velocity Stress Intensity Curves for Stress Corrosion Cracking of GRP. Advances in Fracture Mechanics, Proceedings of the 6th International Conference on Fracture, New Delhi, India, December 4-10, pp. 3053-3060.

14. Sheard, P.A., and Jones, F.R. (1986). The Effect of Environment on Stress Corrosion of Single E-Glass Filaments and the Nucleation of Damage in Glass Fibre Reinforced Plastics. Proceedings of FRC '86, Inst. Mech. Engr. paper C38/86, pp. 63-68.

15. Jones, F.R. (1994). Chapter 6.5 Stress Corrosion Cracking of GRP. Handbook of Polymer-Fibre Composites, F.R. Jones, Ed., Polymer Science and Technology Series, Longman Scientific & Technical Publishers, Longman Group U.K. Ltd., Essex, England, pp. 379-388.

16. Rawles, J.D., Roscow, J.A., and Phillips, M.G. (1990). The Effect of Transient Overloads on the Long Term Performance of Glass Fibre Reinforced Polymer (GFRP) Pipes for Power Station Cooling Water Systems. The 1990 Pressure Vessels and Piping Conference, Nashville, Tennessee, June 17-21, American Society of Mechanical Engineers, PVP Vol. 196, pp. 17-21.

17. Crowther, M.F., Wyatt, R.C., and Phillips, M.G. (1989). Creep-Fatigue Interactions in Glass Fibre/Polyester Composites. Composites Science and Technology, Vol. 36, pp. 191-210.

18. Moore, R.H., and Dillard, D.A. (1990). Time-dependent Matrix Cracking in Cross-ply Laminates. Composites Science and Technology, Vol. 39, pp. 1-12.

19. Tavakoli, S.M., and Phillips, M.G. (1991). Compatibility and Durability in Glass/Phenolic Laminating Systems. ICCM8, The 8th International Conference on Composite Materials.

20. Phillips, M.G. (1983). Prediction of Long-term Stress-Rupture Life for Glass Fibre-Reinforced Polyester Composites in Air and in Aqueous Environments. Composites, Vol.14, No. 3, July, pp.270-275.

21. Dillard, D.A., and Brinson, H.F. (1983). A Numerical Procedure for Predicting Creep and Delayed Failures in Laminated Composites. Long-Term Behavior of Composites, ASTM STP 813, T.K. O'Brien, Ed., American Society for Testing and Materials, Philadelphia, PA, pp. 23-37.

22. Reifsnider, K.L., Stinchcomb, W., and Osiroff, R. Modeling of Creep Rupture Mechanisms in Composite Material Systems.

23. Reifsnider, K.L., and Stinchcomb, W. (1986). A Critical Element Model of the Residual Strength and Life of Fatigue-Loaded Composite Coupons. Composite Materials: Fatigue and Fracture, ASTM STP 907, H.T. Hahn (Ed.), American Society for Testing and Materials, Philadelphia, PA, pp. 298-303.

24. Reifsnider, K.L., (1991). Performance Simulation of Polymer-Based Composite Systems. In Durability of Polymer-Based Composite Systems for Structural Applications, A.H. Cardon and G. Verchery (Eds.), Elsevier Applied Science, New York, pp. 3-26.

25. Reifsnider, K.L., (1992). Use of Mechanistic Life Prediction Methods for the Design of Damage Tolerant Composite Material Systems. ASTM STP 1157, American Society for Testing and Materials, Philadelphia, PA, pp. 205-223.

26. Reifsnider, K.L. (1997). Some Fundamental Aspects of the Fatigue and Fracture Response of Composite Materials. Proceedings of the 14th Annual Meeting, Society of Engineering Science, G.C. Sih, Ed., Recent Advances in Engineering Science, pp. 373-384.

27. Rosen, B.W. (1972). A Simple Procedure for Experimental Determination of the Longitudinal Shear Modulus of Unidirectional Composites. Journal of Composite Materials, Vol. 6, pp. 552-554.

28. O'Brien, T.K., Salpekar, S.A. (1993). Scale Effects on the Transverse Tensile Strength of Graphite/Epoxy Composites. Composite Materials: Testing and Design (Eleventh Volume), ASTM STP 1206, E.T. Camponeschi, Jr., Ed., American Society for Testing and Materials, Philadelphia, pp. 23-52.

29. Stinchcomb, W.W., Reifsnider, K.L., Yeung, P., and Masters, J. (1981). Effect of Ply Constraint on Fatigue Damage Development in Composite Materials. Fatigue of Fibrous Composite Materials, ASTM STP 723, American Society for Testing and Materials, pp. 64-84.

Table 1. Elastic and Strength Properties of E-glass/913
from Quasi-Static Tensile Tests in Universal Test Machine

stacking sequence	spec. #	width (mm)	thickness (mm)	Young's modulus (GPa)	Failure Load (kN)	Tensile Strength (MPa)
$[0]_8$	UB-3	25.51	1.17	44.3	25.95	869.4
	UB-4	25.22	1.17	47.9	25.15	852.3
	UB-10	25.60	1.17	45.7	25.90	864.7
$[0/90/+45/-45]_S$	Q8-6	25.14	1.13	21.4	8.78	309.1
	Q8-8	25.26	1.12	21.6	9.18	324.5
$[0_2/90_2/+45_2/-45_2]_S$	Q16-3	25.15	2.32	22.9	18.18	311.6
	Q16-5	25.29	2.28	21.7	17.66	306.3

Table 2. Elastic Properties of E-glass/913 from Creep Test Data

stacking sequence	spec. #	width (mm)	thickness (mm)	Exx (GPa)	E22 (GPa)	G12 (GPa)
$[90]_8$	U90-6	24.04	1.00	14.1	14.1	–
	U90-7	23.92	0.99	15.2	15.2	–
	U90-8	23.95	1.01	13.6	13.6	–
	U90-10	23.90	1.00	13.4	13.4	–
$[+45/-45/+45/-45]_S$	S-1	25.24	1.19	23.5	–	8.95
	S-3	25.16	1.21	14.7	–	5.58
	S-4	25.34	1.18	15.9	–	6.04
	S-6	25.15	1.22	14.4	–	5.49
	S-7	25.28	1.16	19.3	–	7.32

Table 3. Stress-Rupture Life Results

stacking sequence	spec. #	Area (mm^2)	Applied Load (kN)	Applied Stress (MPa)	Young's Modulus (GPa)	Time to Failure (hours)
$[0]_8$	UA-4	27.08	16.39	605	na	0.13
$[0]_2$	U2-1	8.42	1.683	200	na	67.0
	U2-2	7.00	1.750	250	46.2	12.2
	U2-3	7.65	1.148	150	na	1701*
	U2-4	8.43	na	na	na	na
	U2-5	7.28	1.092	150	na	1700*
	U2-6	7.80	1.561	200	45.5	88.8
	U2-7	7.95	1.391	175	na	1600*
	U2-8	7.96	na	na	na	na
	U2-9	6.56	1.475	225	45.0	18.7
	U2-10	9.42	1.884	200	43.2	38.0
$[0/90/+45/-45]_S$	Q8-1	29.33	2.346	80	na	1053*
	Q8-2	28.15	3.604	128	23.0	47.3
	Q8-3	28.89	2.311	80	na	381.9
	Q8-4	29.14	3.264	112	24.9	120.0
	Q8-5	28.79	3.224	112	23.0	72.0
	Q8-7	28.32	3.171	112	22.3	130.3
	Q8-9	30.52	3.907	128	na	25.3
	Q8-10	28.35	3.629	128	na	22.6
$[0_2/90_2/+45_2/-45_2]_S$	Q16-1	53.96	6.690	124	23.77	100.1
	Q16-2	58.21	8.965	154	21.83	13.8
	Q16-4	56.36	6.087	108	23.43	335.8
	Q16-6	55.97	8.619	154	22.33	13.0
	Q16-7	56.47	7.002	124	23.59	59.8
	Q16-8	58.18	7.214	124	22.86	92.3
	Q16-9	58.53	6.322	108	23.49	119.5
	Q16-10	50.67	5.472	108	26.98#	123.0

* no failure, test was interrupted

na data not available

\# specimen was thin (panel edge)

Figure 1. Creep frame with 90° specimen and extensometers installed.

Figure 2(a). Unidirectional specimen showing clamps reinforcing the bonded end tabs. A clear plastic sheet is sealed with Tacky Tape brand of sealing strips to contain acid leaked from the acid cell upon failure of the specimen.

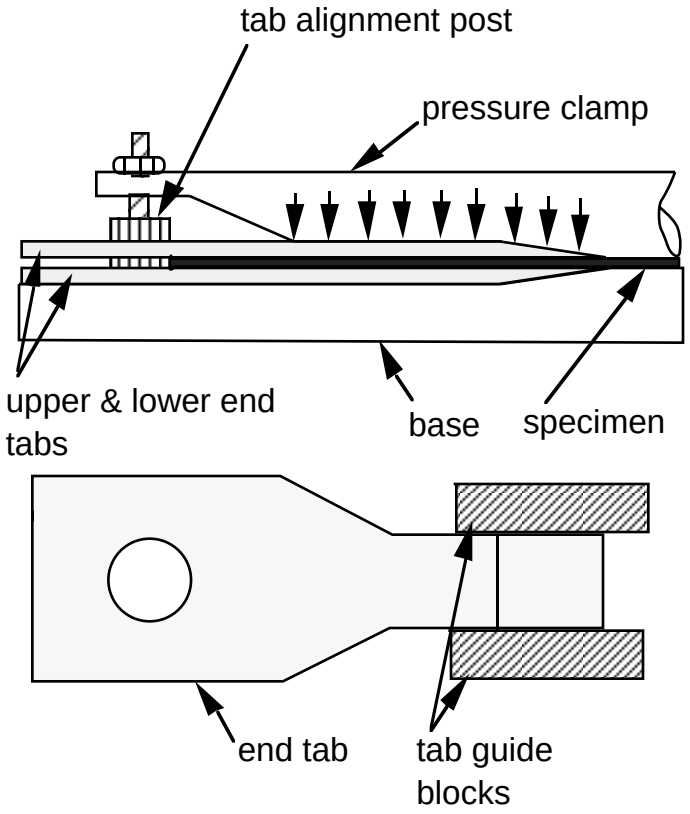

Figure 2(b). Diagram showing a portion of the fixture for aligning end tabs with the specimen. A uniform clamping pressure is applied along the bonded length of the tab (including the chamfered portion). The alignment post centers the holes in the tabs.

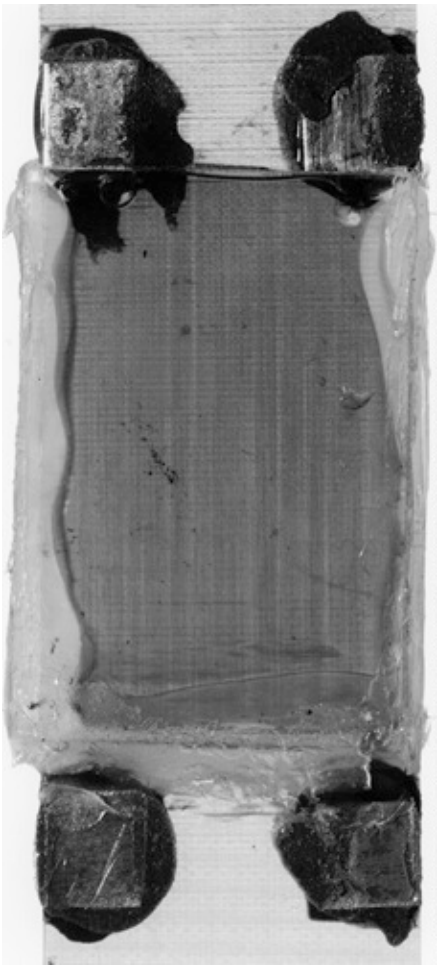

Figure 3. Close-up of the acid cell. The cells are glass slides 37 x 25 mm and are bonded in place, one on each side, with a clear silicon rubber sealant. The specimen edges are completely sealed. The squares of sheet aluminum are bonded using a paste epoxy adhesive and serve as pads for the extensometer screws to bite into.

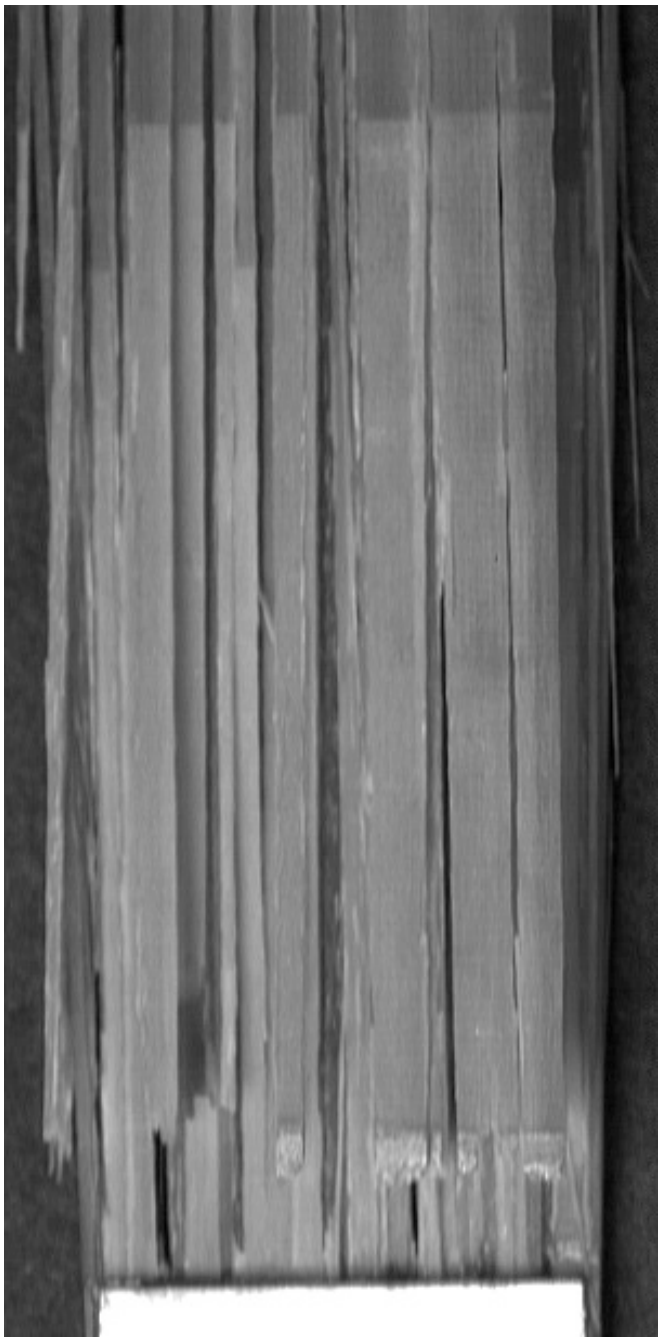

Figure 4(a). Fracture of $[0]_8$ quasi-static tensile specimen. Fracture initiated at the edge, at the grip edge, and proceeded by a repeated sequence of fiber fracture and splitting.

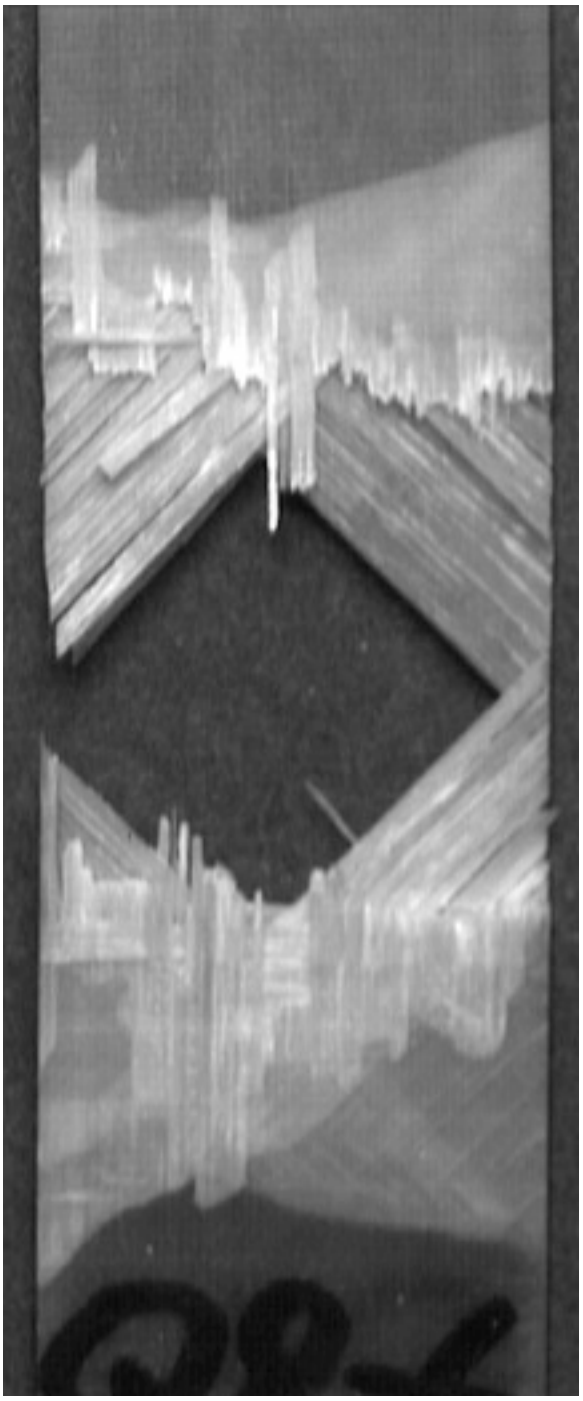

Figure 4(b). Representative fracture profile of a quasi-static tensile test of $[0/90/+45/-45]_s$ E-Glass/913-epoxy laminate. Higher constraint than in 4(a) prevents unrestrained splitting. The irregular profile is due to alternation of fiber bundle fracture and splitting. The 45 degree plies have not fractured, but instead split and shear out. Light areas are delamination.

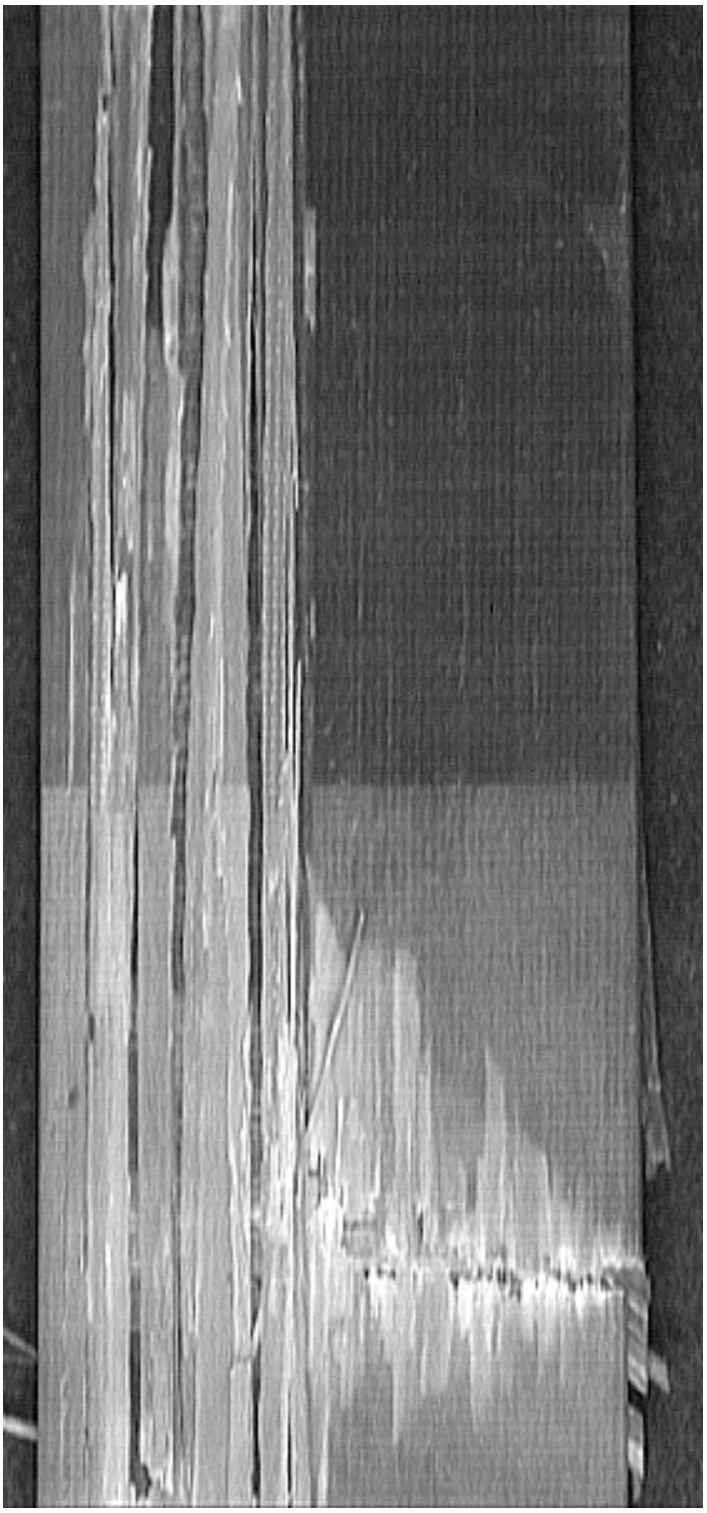

Figure 4(c). Representative fracture profile of a quasi-static tensile test of $[0_2/90_2/+45_2/-45_2]_s$ E-Glass/913-epoxy laminate. Lower constraint of 0° plies causes unrestrained splitting.

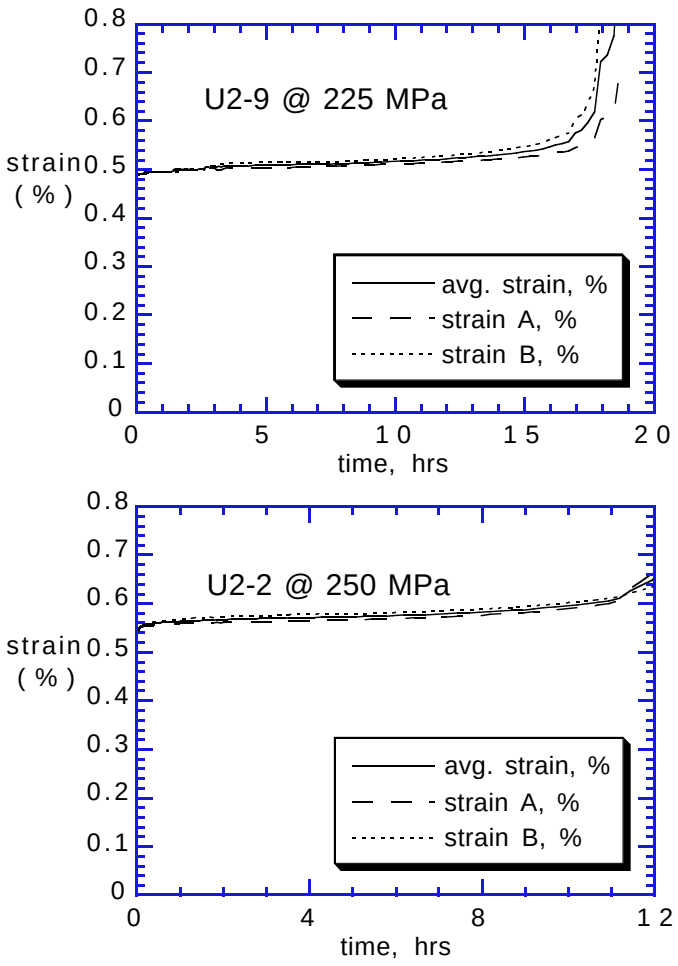

Figure 5. Creep results for constant stress tests of $[0]_2$ E-glass/913-epoxy in 0.01 molar HCl acid bath.

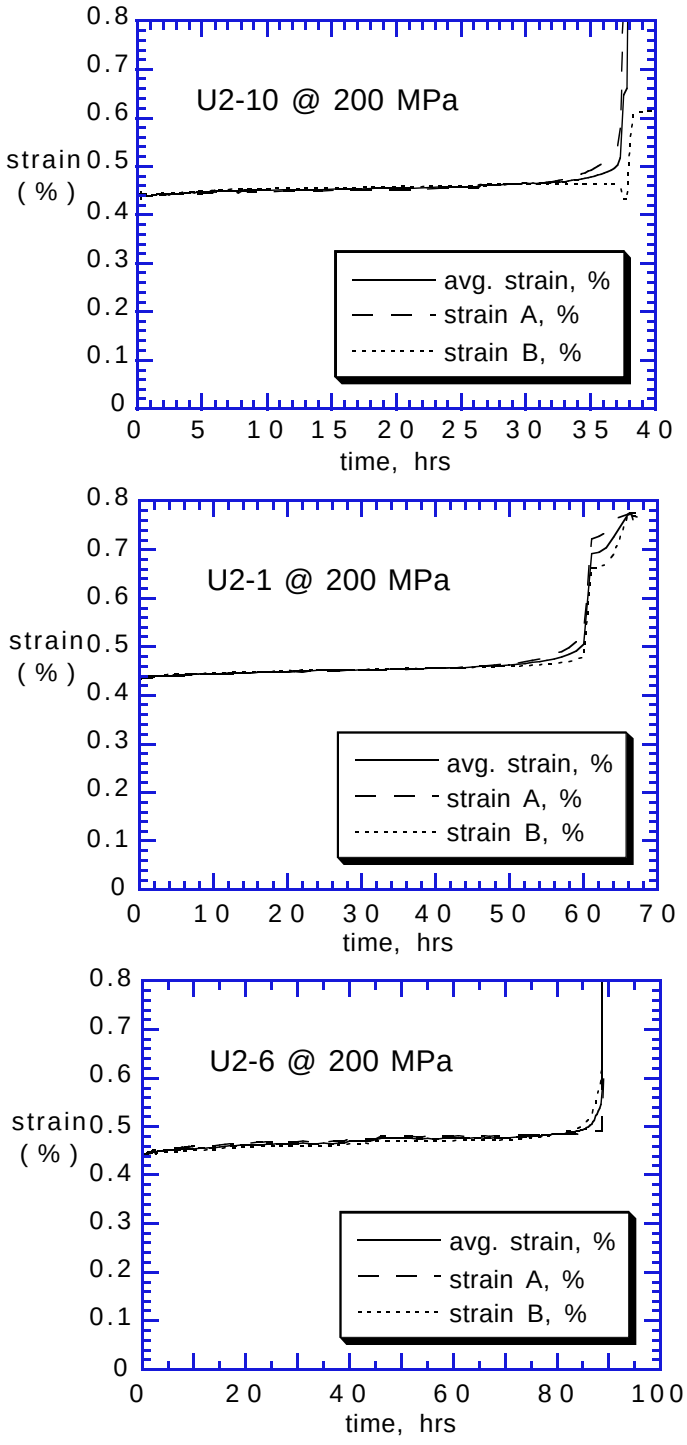

Figure 6. Creep results for 200 MPa constant stress tests of $[0]_2$ E-glass/913-epoxy in 0.01 molar HCl acid bath.

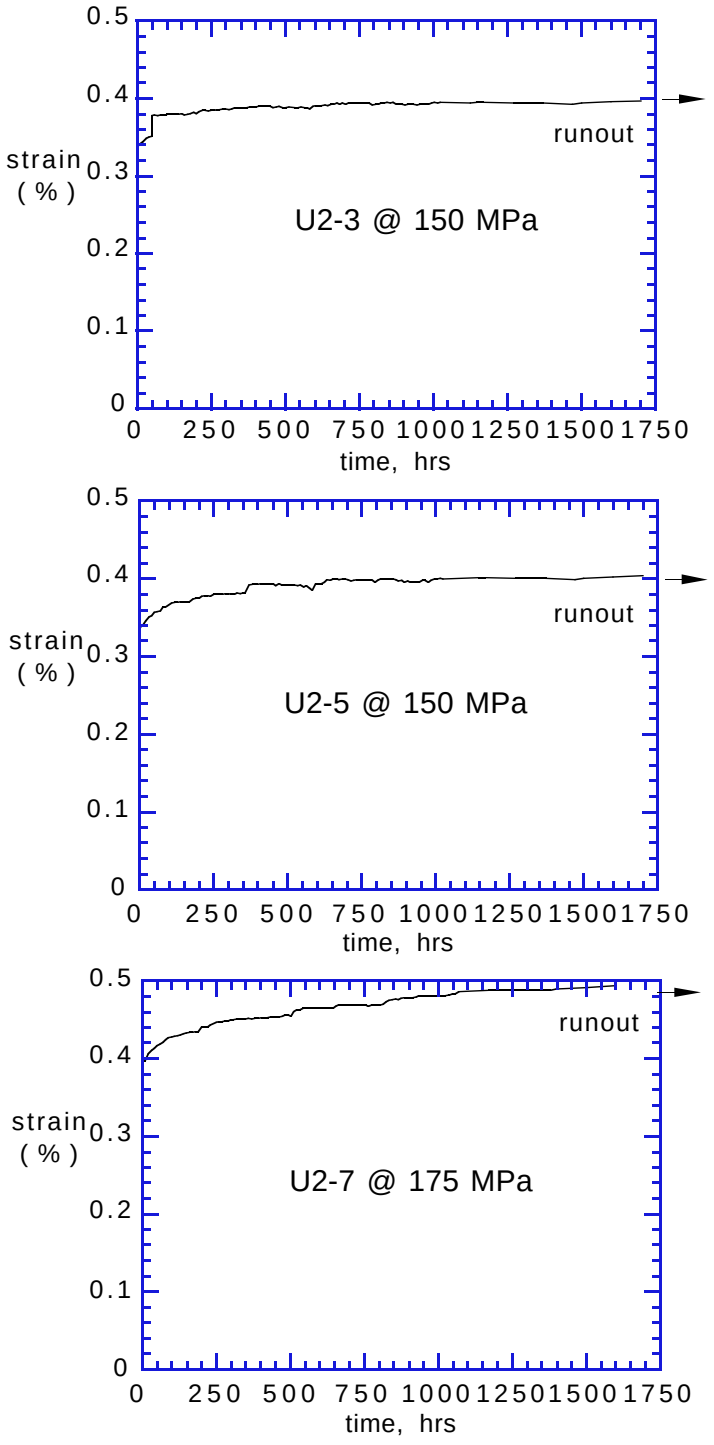

Figure 7. Creep results for constant stress tests of $[0]_2$ E-glass/913-epoxy in 0.01 molar HCl acid bath. Tests were stopped before failure. No cracks had formed.

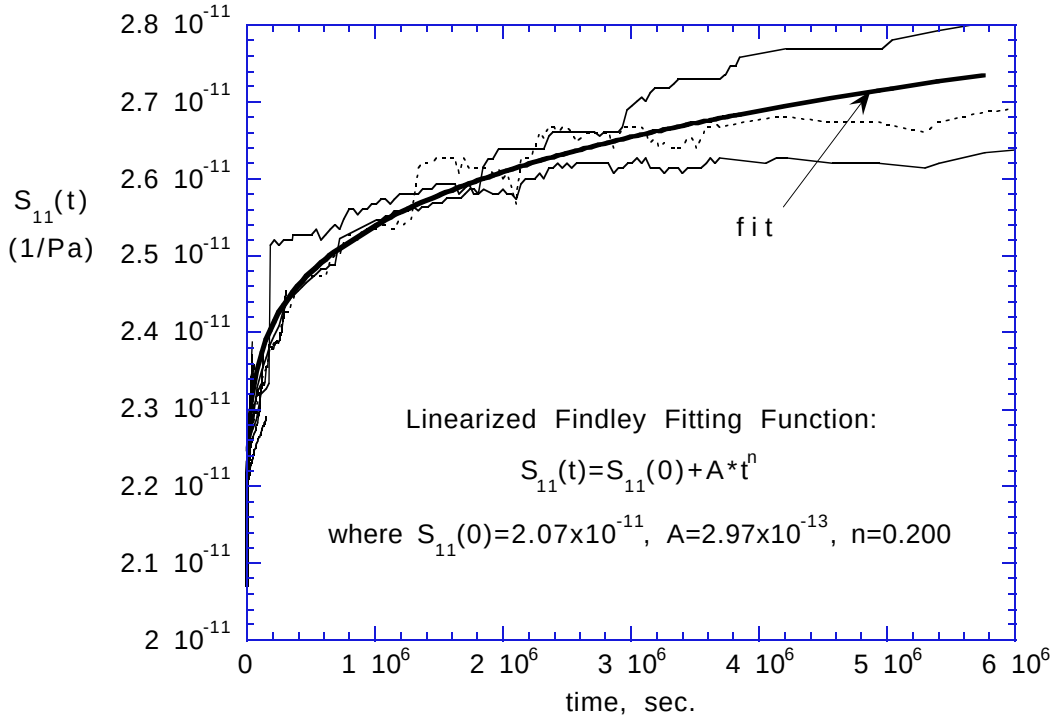

Figure 8. The linearized Findley fitting function is fit to experimentally determined $S_{11}(t)$ compliance vs. time data for unidirectional $[0]_2$ E-glass/913-epoxy immersed in a 0.01 molar hydrochloric acid bath. Heavy line is the fit, light lines are data.

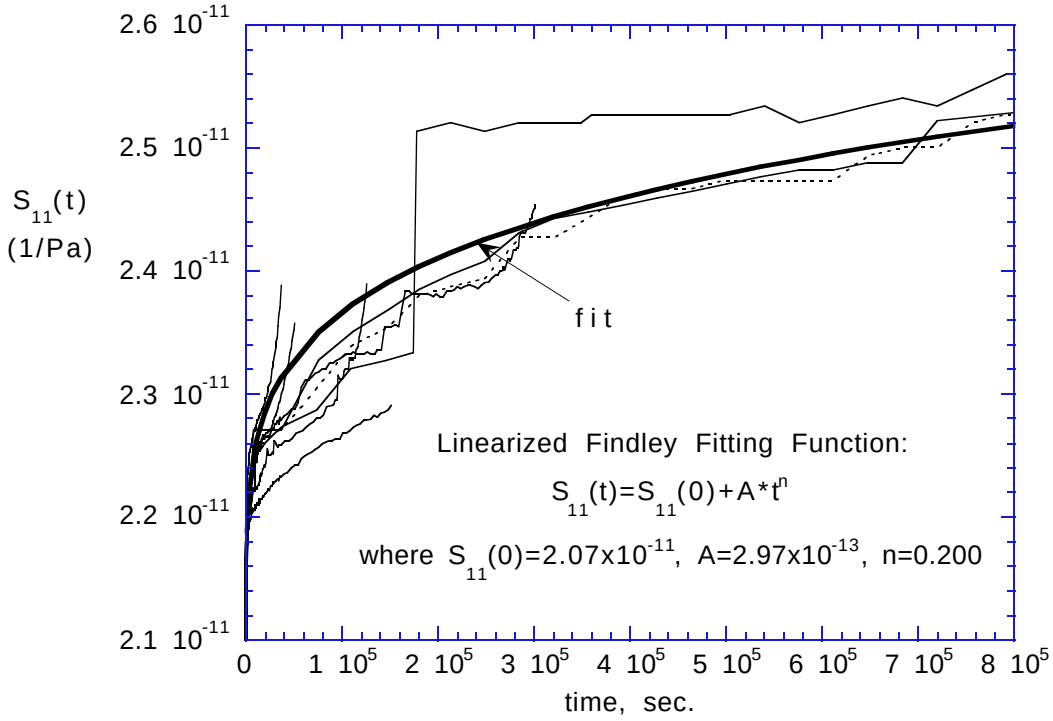

Figure 9. Examination of quality of fit early in the life. Heavy line is the fit, light lines are data. Where data turn upward at the end of their life is compliance change due to accumulation of damage. Damage influences compliance for a significant portion of the life of the highly stressed specimens, but may be ignored when characterizing the low-stress long-life specimens. Hence, only the effect of matrix stress relaxation on compliance is accounted for.

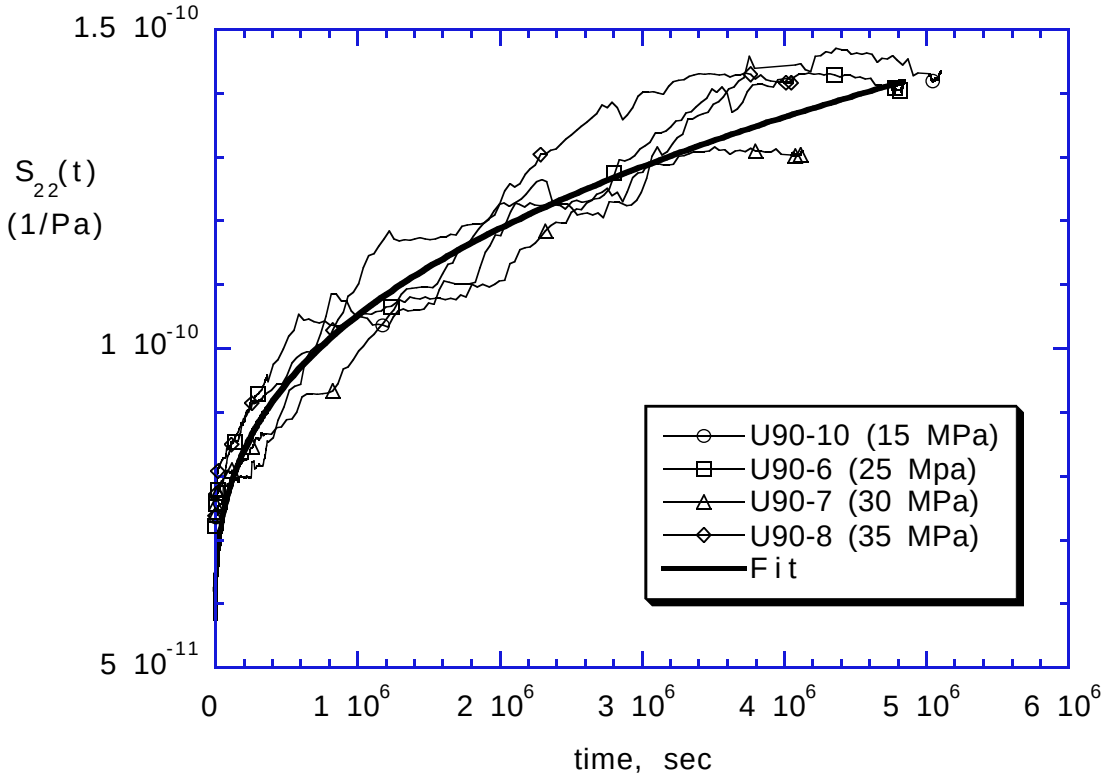

Linearized Findley Fitting Function:

$S_{22}(t)=S_0+A*t^n$

where $S_0=5.62x10^{-11}$, $A=3.629x10^{-13}$, $n=0.355$

Figure 10. Linearized Findley fitting funtion (heavy line) fit to experimentally determined $S_{22}(t)$ (transverse compliance) vs. time data (light lines). No apparent stress dependence.

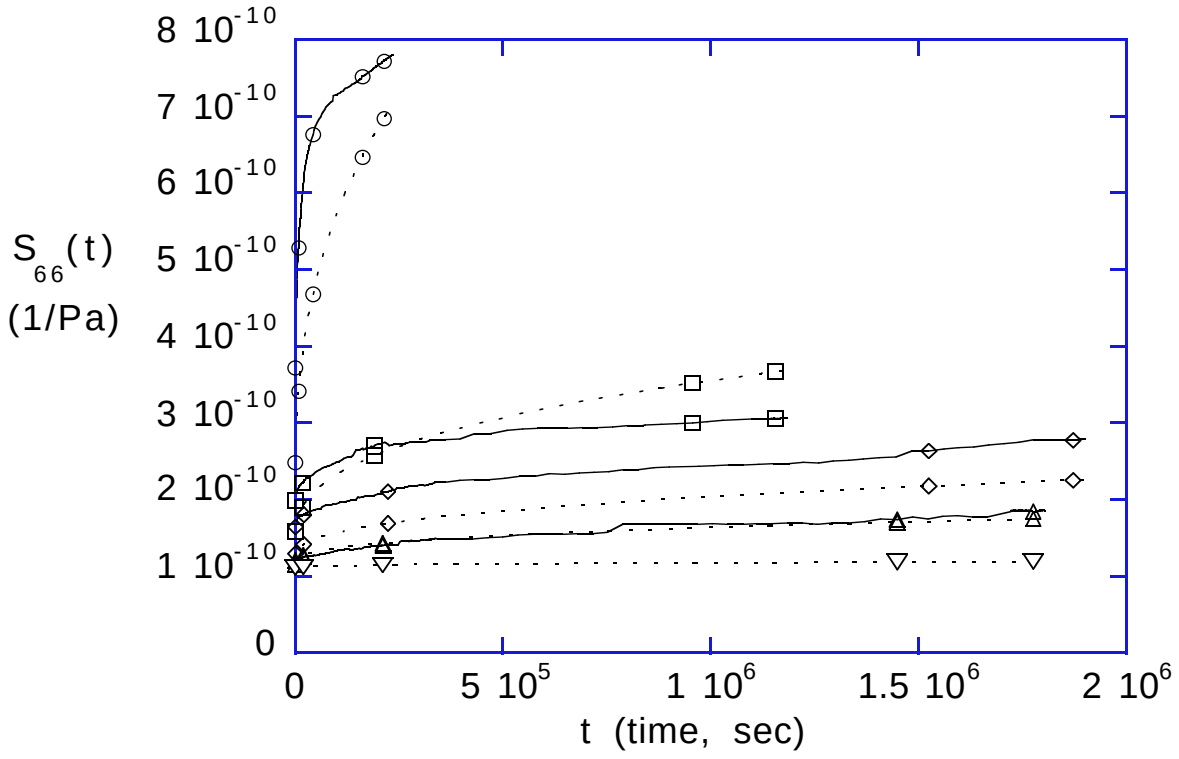

Schapery's fit: $S_{66}(\sigma,t)= S_{66}(0)*(1+g\sigma^2)+m(1+f\sigma^2)t^2$

$g=2.8x10^{-16}$ $m=12.36x10^{-15}$ $f=1.0x10^{-13}$ $n=0.37$

Figure 11. Schapery's quadratic fitting function (dashed lines) is fit to experimentally determined $S_{66}(t)$ (shear compliance) vs. time data (solid lines) from $[+45/-45]_{2S}$ E-glass/913-epoxy tensile creep tests. Stress dependency, σ, is included.

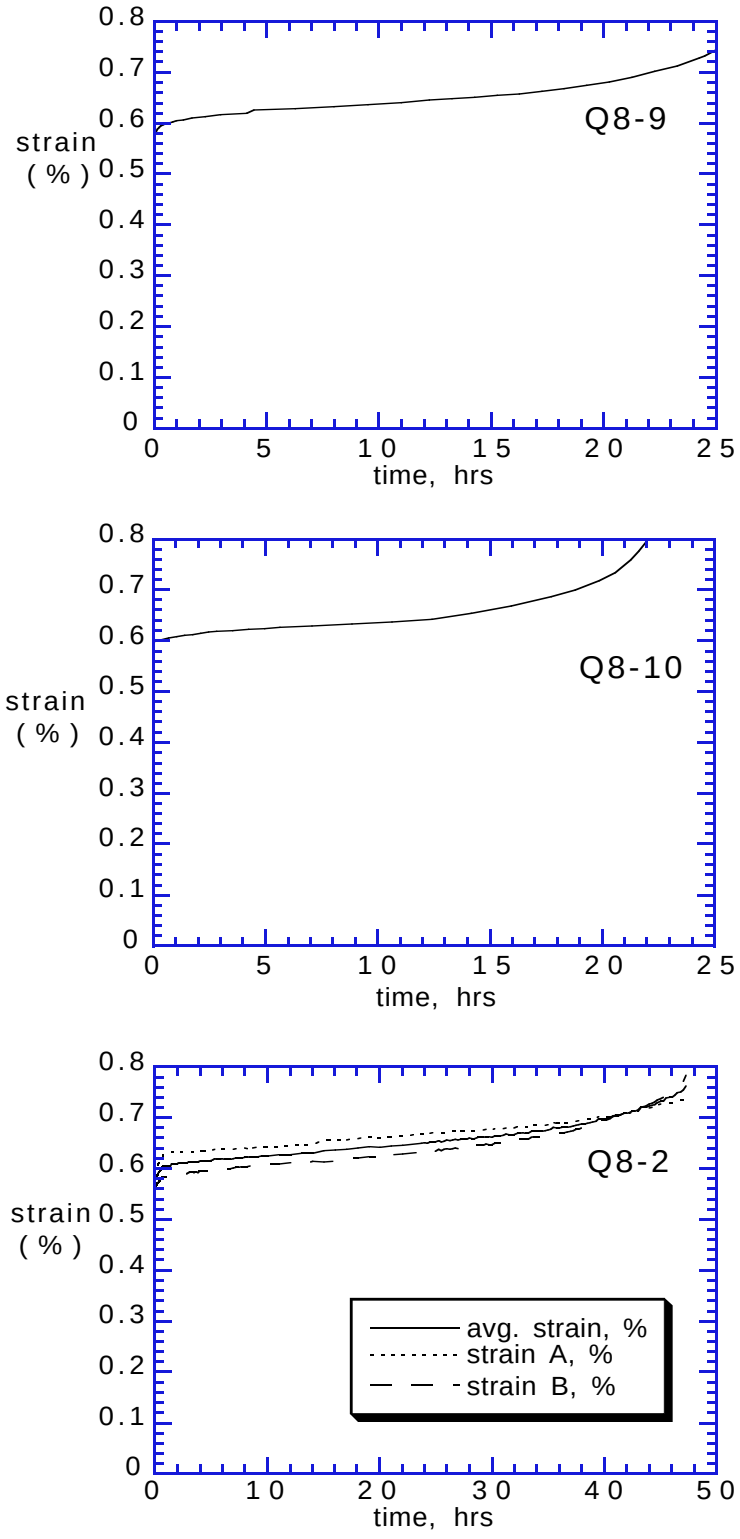

Figure 12. Creep results for 128 MPa constant stress tests of $[0/90/+45/-45]_s$ E-glass/913-epoxy in 0.01 molar HCl acid bath.

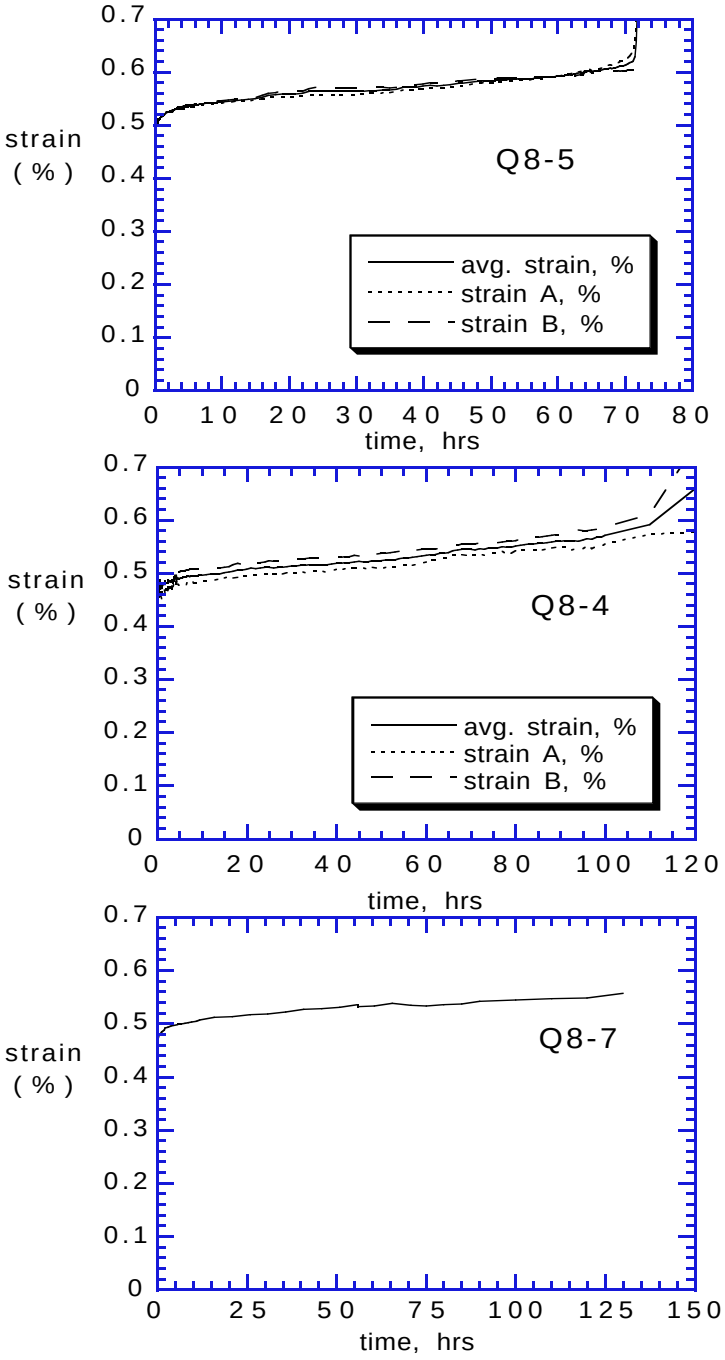

Figure 13. Creep results for 112 MPa constant stress tests of $[0/90/+45/-45]_s$ E-glass/913-epoxy in 0.01 molar HCl acid bath.

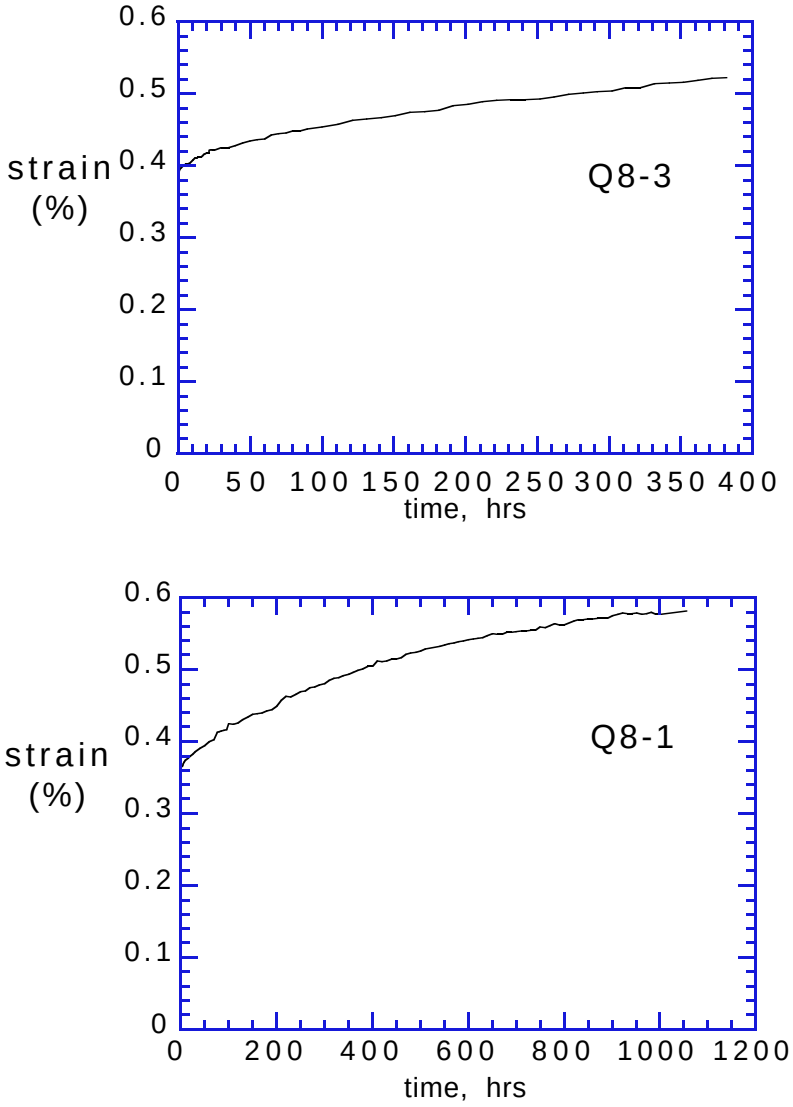

Figure 14. Creep results for 80 MPa constant stress tests of $[0/90/+45/-45]_s$ E-glass/913-epoxy in 0.01 molar HCl acid bath.

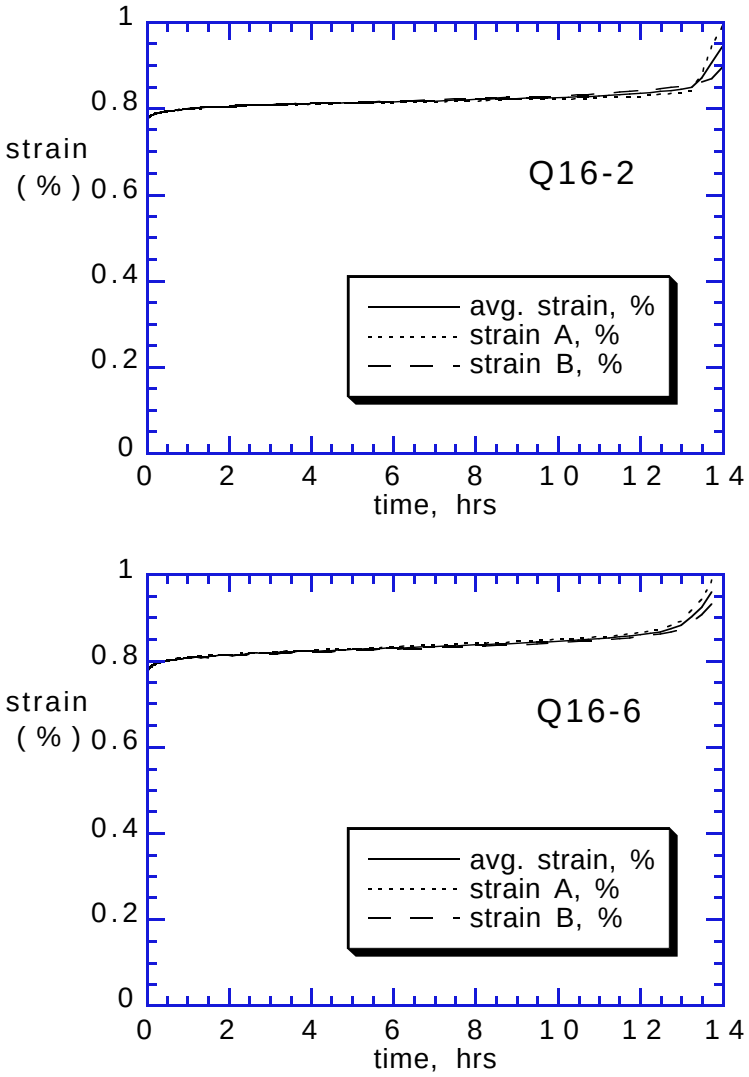

Figure 15. Creep results for 154 MPa constant stress tests of $[0_2/90_2/+45_2/-45_2]_s$ E-glass/913-epoxy in 0.01 molar HCl acid bath.

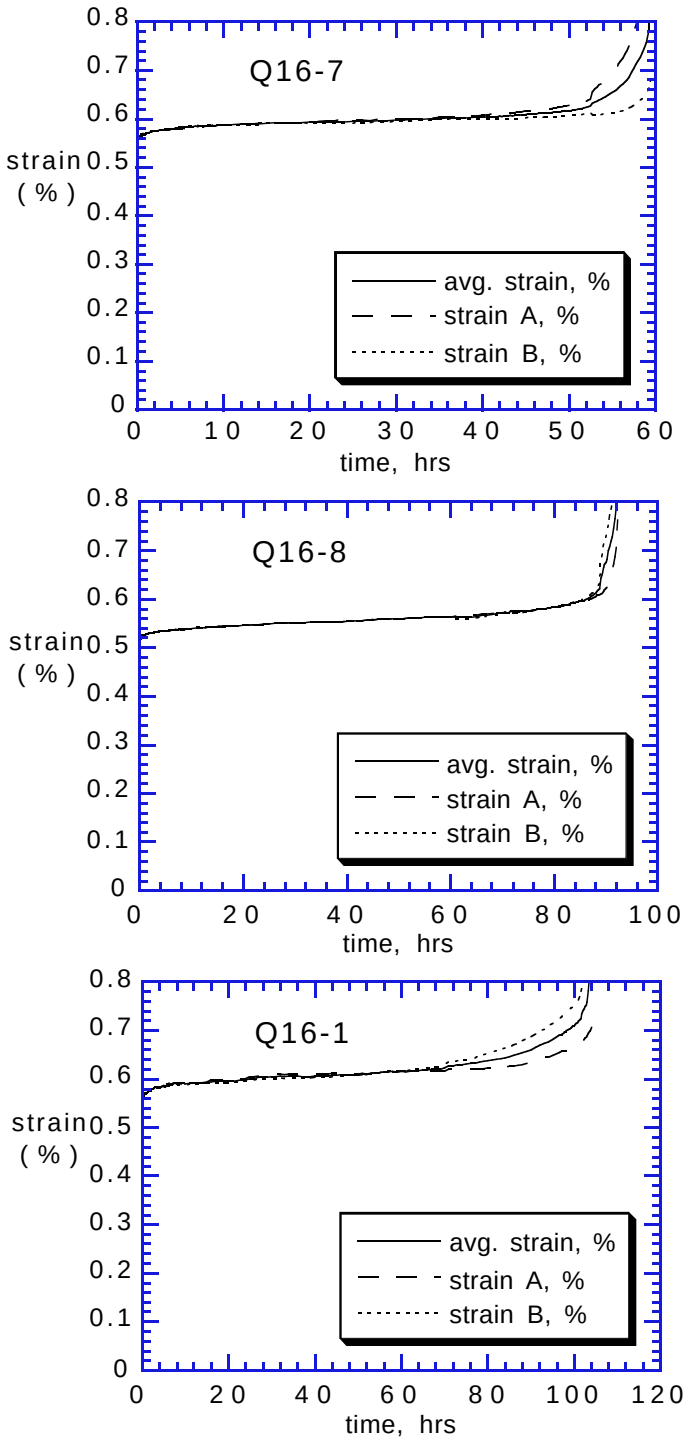

Figure 16. Creep results for 124 MPa constant stress tests of $[0_2/90_2/+45_2/-45_2]_s$ E-glass/913-epoxy in 0.01 molar HCl acid bath.

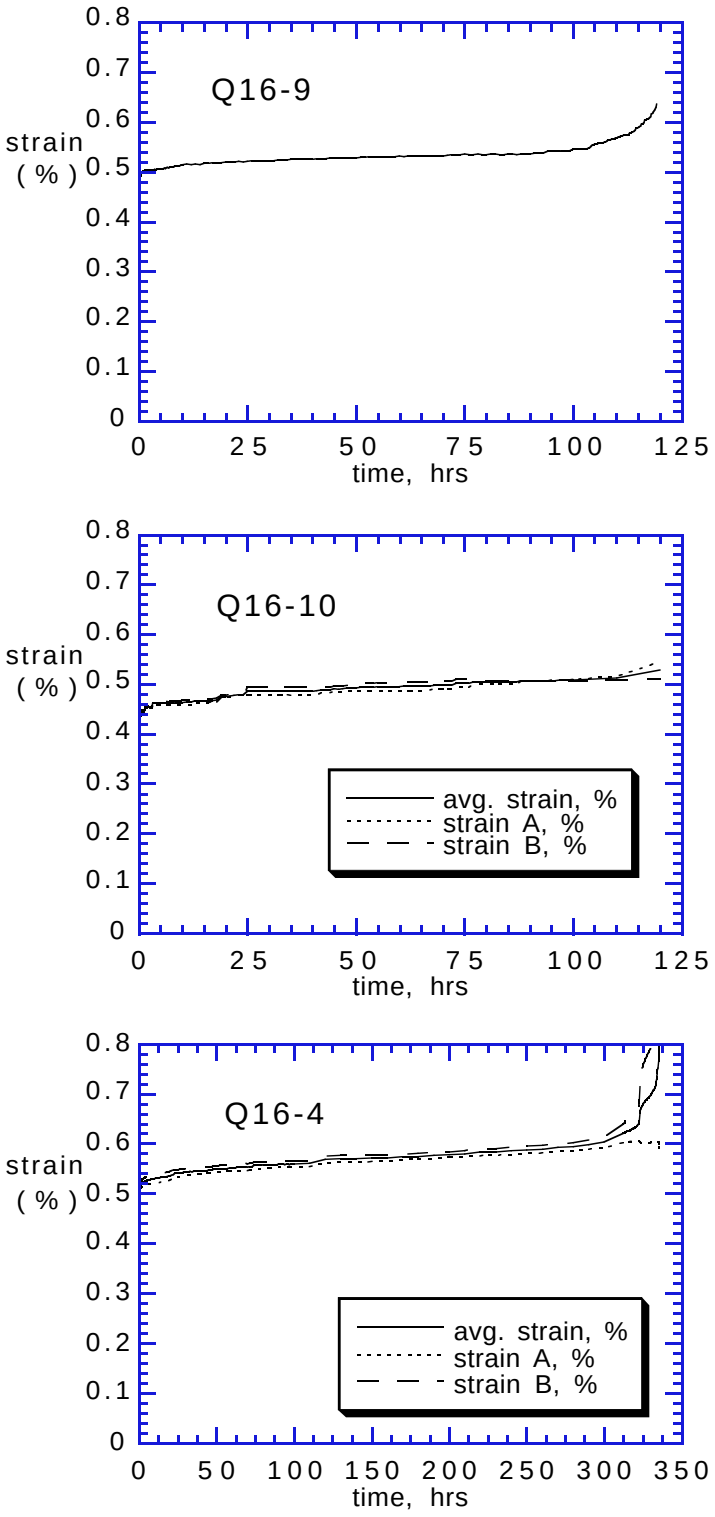

Figure 17. Creep results for 108 MPa constant stress tests of $[0_2/90_2/+45_2/-45_2]_s$ E-glass/913-epoxy in 0.01 molar HCl acid bath.

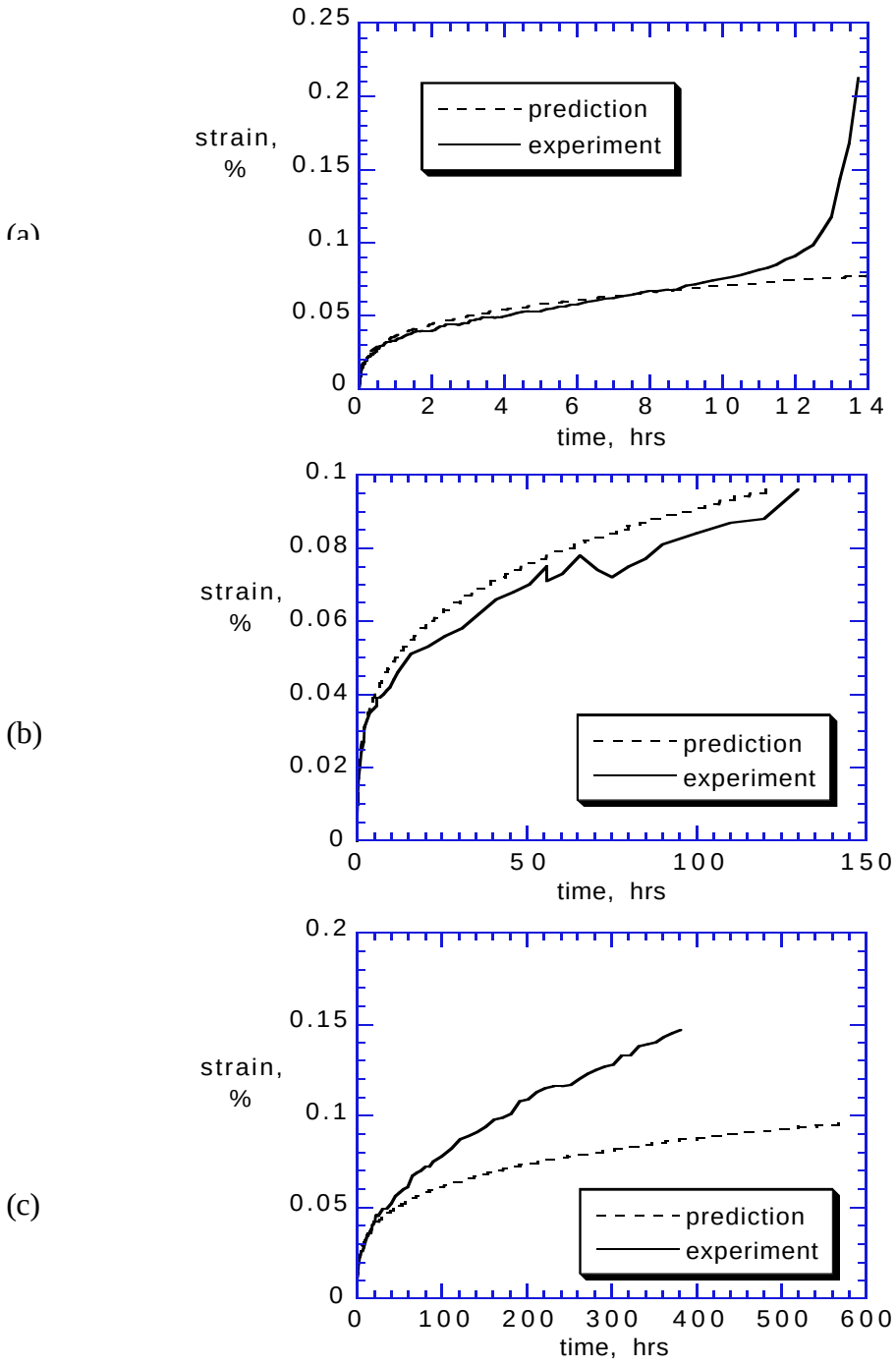

Figure 18. Predicted and experimental creep vs. time response of quasi-isotropic layup. In (a) and (b) agreement is good, until stress-corrosion cracks radically increase strain. In (c) the error is substantial, and is likely because at long times the effects of moisture uptake on compliance and expansion become significant.

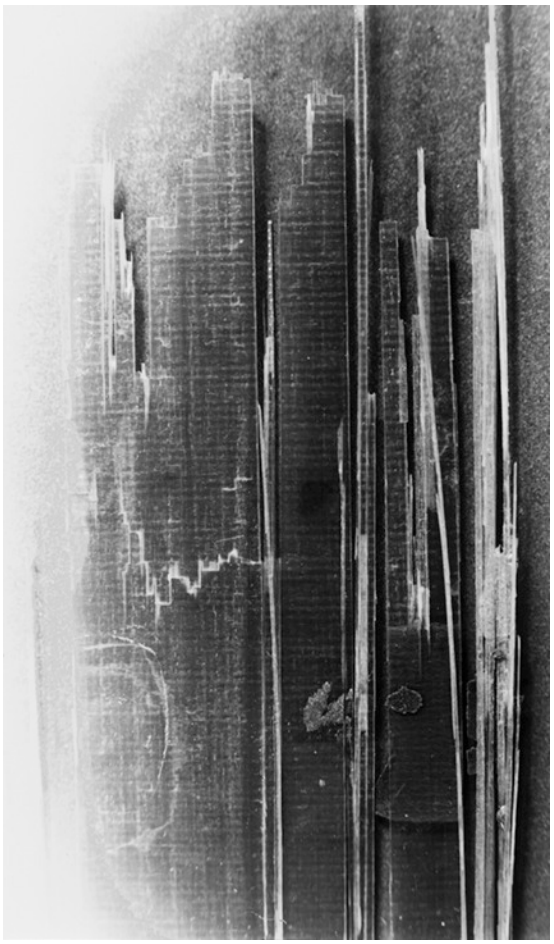

Figure 19. Representative fracture profile of stress-ruptured $[0]_2$ E-Glass/913-epoxy having a higher stress (225 MPa), and shorter life (18.7 hours). The irregular profile is due to a large number of small cracks forming accompanied by splitting which arrests their growth.

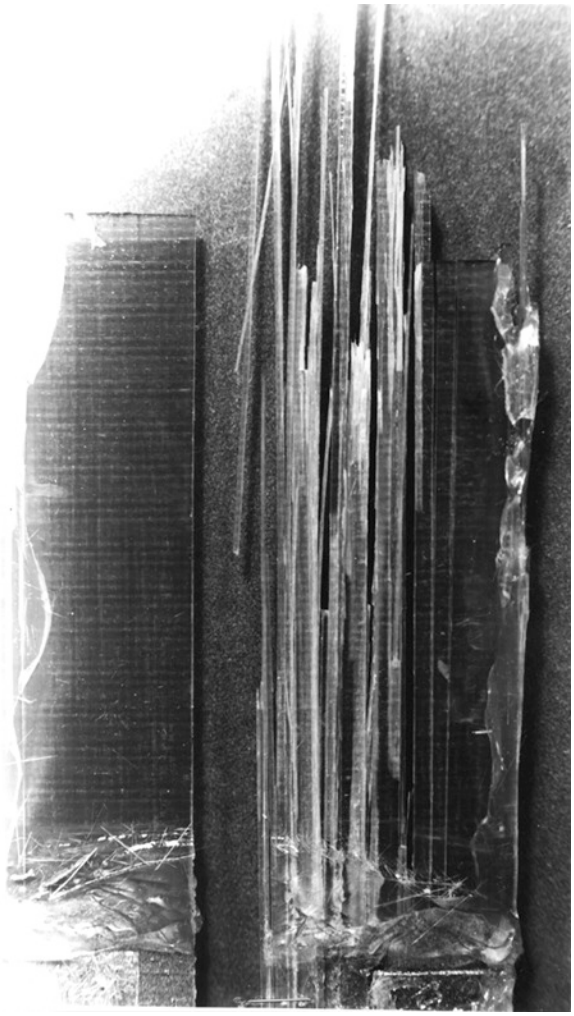

Figure 20. Representative fracture profile of stress-ruptured $[0]_2$ E-Glass/913-epoxy having a lower stress (185 MPa), and longer life (41 hours). The mixed profile is due to two long cracks growing without forming splits, then the highly stressed remaining cross-section fails much like the that of Figure 19. (shows U2-9).

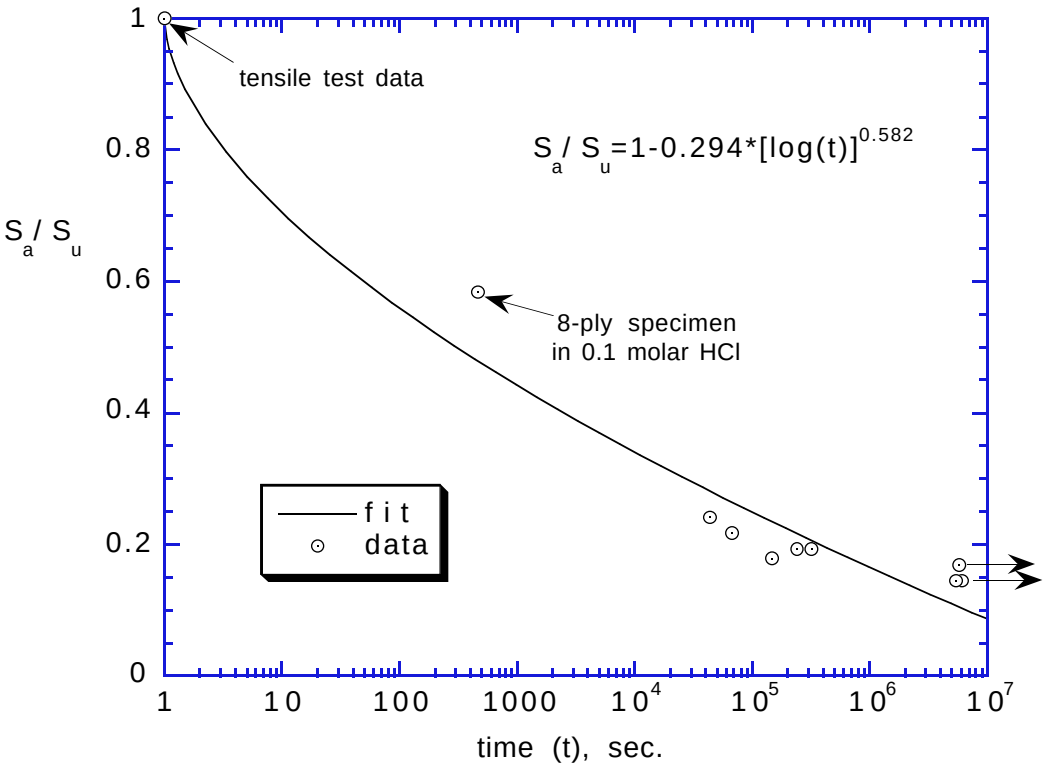

life function: $F_a = \frac{S_a}{S_u} = A + B[log(t)]^p$

fit parameters: A=1 B=-0.294 p=0.583

Figure 21. Life versus time response of E-glass/913 in 0.01 molar HCl. Fit (solid line) to stress-rupture life data (circles).

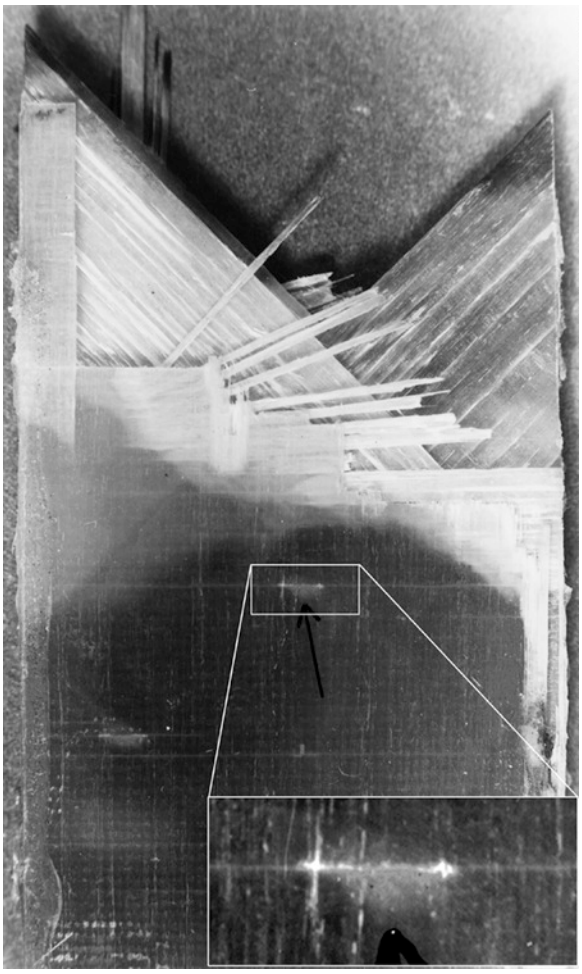

Figure 22. Representative fracture profile of stress-ruptured $[0_2/90_2/+45_2/-45_2]_s$ E-Glass/913-epoxy having a higher stress (154 MPa), and shorter life (13.0 hours). The stress-corrosion cracks grow across much of the laminate, with no attack to the underlying layers, in particular the 45's are intact. There are two prominent stress-corrosion cracks visible below the fracture zone (one is magnified). Width-spanning 90° cracks then appeared, accompanied by an oval delamination at the 0/90 interface around the zone having the 0° crack. There were 90° cracks only where 0° stress-corrosion cracks preexist.

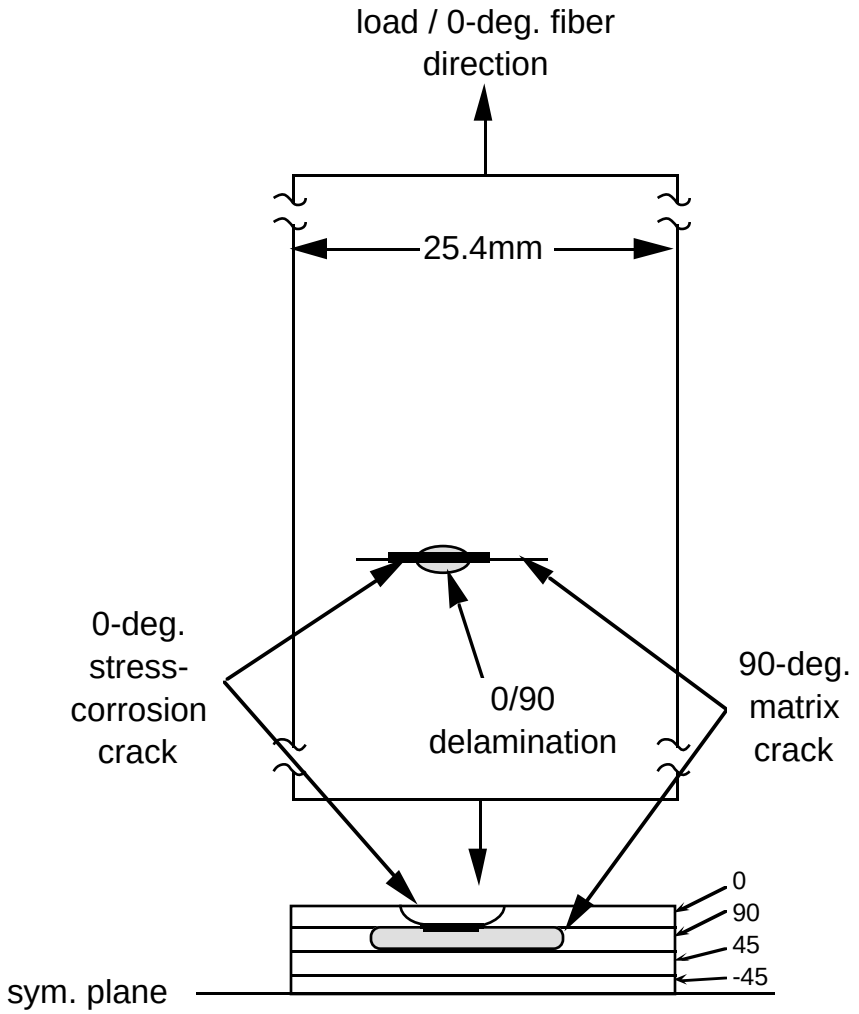

Figure 23. Schematic of the formation of a stress-corrosion crack (thick line) in the surface 0°-ply, and the subsequent appearance of a 0/90 delamination (shaded oval in upper Figure) and a 90°-crack (thin line). This sequence was typical because the loading was below that to initiate 90° matrix cracks.

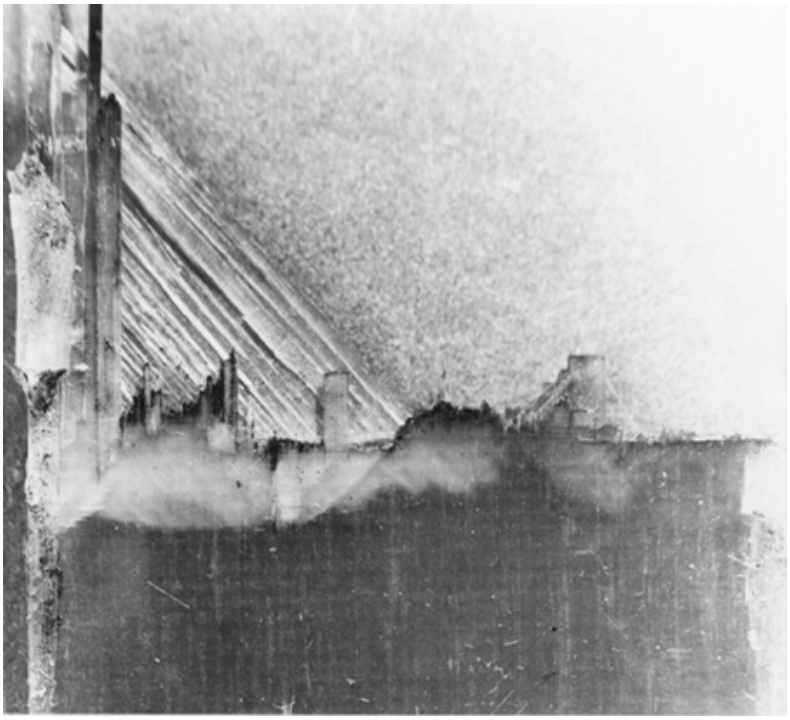

Figure 24. Representative fracture profile of stress-ruptured $[0/90/+45/-45]_s$ E-Glass/913-epoxy having a lower stress (112 MPa), and longer life (130.3 hours). The stress-corrosion cracks grow across much of the laminate, and clean through about 40% of the width. Only a portion of the midplane -45° plies have not fractured. The light area just below the fracture line is a delamination.

Figure 25. Representative fracture profile of stress-ruptured $[0_2/90_2/+45_2/-45_2]_s$ E-Glass/913-epoxy having a lower stress (108 MPa), and shorter life (119 hours). The stress-corrosion cracks grow across about 20% of the laminate, while the 0° plies cracked across much of the width before final separation.

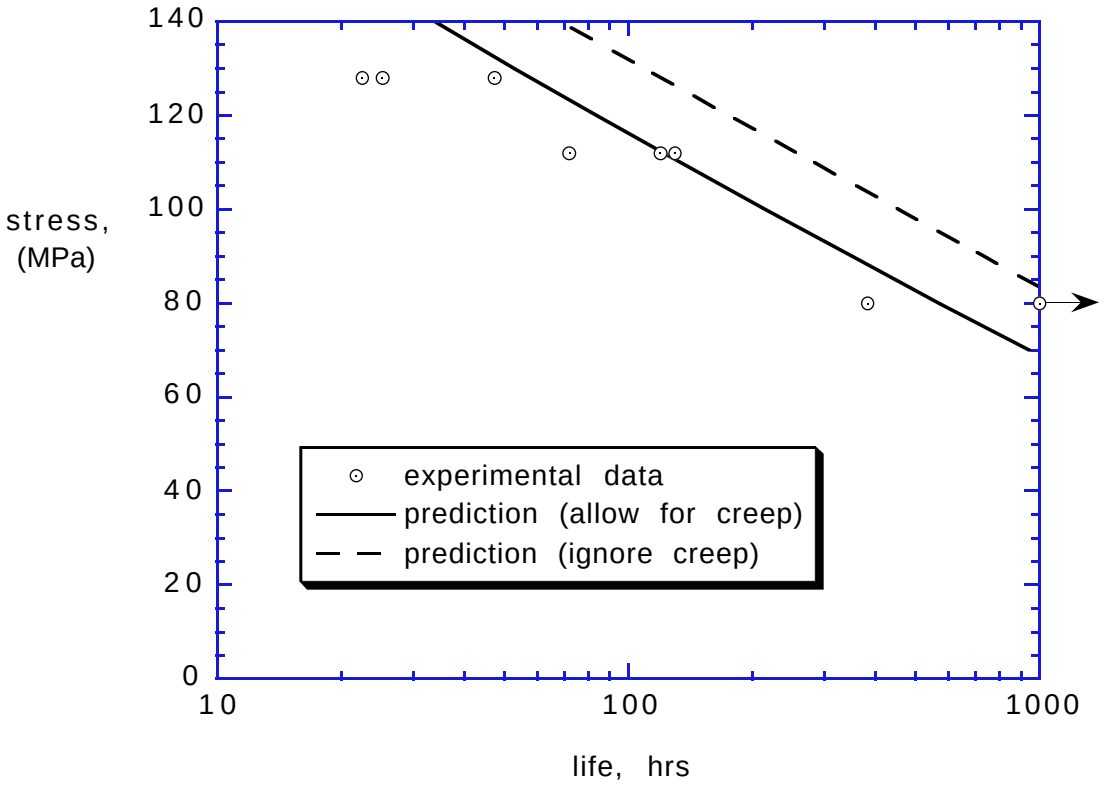

Figure 26. Prediction of the stress-rupture life of a $[0/90/+45/-45]_S$ quasi-isotropic laminate of E-glass/913-epoxy under tension and immersed in an 0.01 molar hydrochloric acid bath. If stress-relaxation (creep) is ignored, life is overpredicted.

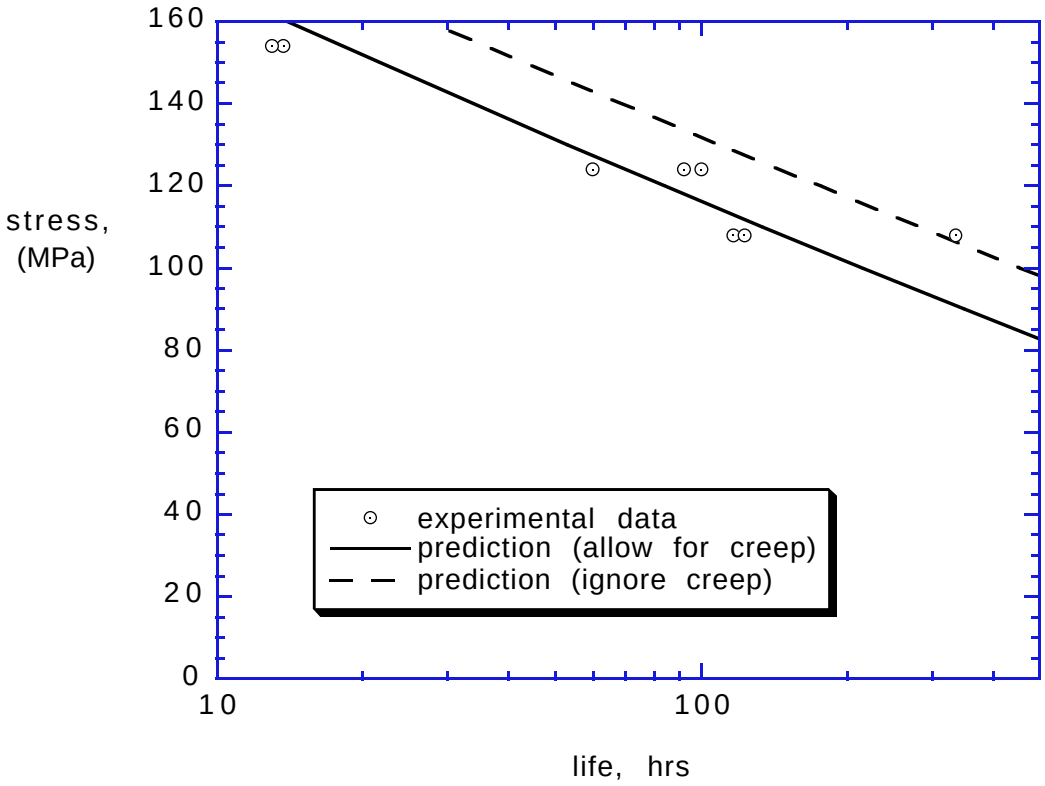

Figure 27. Prediction of the stress-rupture life of a $[0_2/90_2/+45_2/-45_2]_S$ quasi-isotropic laminate of E-glass/913-epoxy under tension and immersed in an 0.01 molar hydrochloric acid bath. If stress-relaxation (creep) is ignored, life is overpredicted.

Appendix. Stress-Rupture Life FORTRAN Code.

```
PROGRAM  LIFE

C     COMPOSITE STRESS-RUPTURE LIFE ANALYSIS

C     J. Andre Lavoie
C     Department of Engineering Science & Mechanics
C     Virginia Polytechnic Institute & State University



      character*40 name(10)
      integer tmax,plies,nomatl,angles,noang,stack
       REAL JVAR, P, tlapse
      double precision matpro,DT,N(3),M(3), PRNSTR(3,151),
     $QBAR,SBAR,ZCOORD,CTE,T,TINV,
     $FR, FA1, FA2, SA1, SA2, SU, TAU1, TAU2, DTAU,
     $A, B, DN, BIGN1, BIGN2, INTGRL, crpstr

       COMMON QBAR(3,3,150),MATPRO(10,12),STACK(150,2),PLIES,SBAR(3,3),
     $   ANGLES(50),ZCOORD(151),CTE(3,150),T(3,3,150),TINV(3,3,150)



C  MATPRO(i,j) contains the material properties used by CLT:
C  (i is the material number, and is usefull for specifying
C   individual laminae for degrading)

C MATPRO(i,1) = E1
C MATPRO(i,2) = E2
C MATPRO(i,3) = G12
C MATPRO(i,4) = Nu12
C MATPRO(i,5) = ply thickness
C MATPRO(i,6) = cte1
C MATPRO(i,7) = cte2
C MATPRO(i,8) = Xt
C MATPRO(i,9) = Xc
C MATPRO(i,10) = Yt
C MATPRO(i,11) = Yc
C MATPRO(i,12) = S



C-----------------------------------------------------------------
C  all results are printed to this file:

      OPEN(unit=6,file='LIFE.out',status='unknown')

C-----------------------------------------------------------------
```

```
C  Initial, undamaged material properties, # of plies, # of materials,
C  and stacking sequence are read from a data file on disk.

      call DATA(plies,nomatl,angles,noang,matpro,name,stack,N,M,DT)

      WRITE(*,*) 'ENTER THE TENSILE FORCE RESULTANT (in N/m):'
      READ(*,*) N(1)
      WRITE(*,*) 'ENTER STEP SIZE (in seconds):'
      READ(*,*) DN

C-----------------------------------------------------------------------
C The initial transverse and shear moduli, E2 and G12, are assumed the
C same for each ply in the stack.

C     E2= MATPRO(1,2)
C     G12= MATPRO(1,3)

      SU= MATPRO(1,8)

C  These constants define the S-N curve of the fibers:

      A= 1.0D0
      B= -0.29425D0
      P= 0.582
      Jvar= 7
      INTGRL= 0.D0


      CALL CLT(nomatl,noang,N,M,DT,PRNSTR,crpstr)
      SA1= PRNSTR(1,1)
C     WRITE(*,*) PRNSTR(1,3), PRNSTR(2,3), PRNSTR(3,3)
      BIGN1= 10**(((SA1/SU-A)/B)**(1./P))
      TAU1= 0.D0
      FA1= SA1/SU

      write(*,100) Sa1,Su,Fa1
  100 format(1x,'initially:'/1x,'Sa=',e10.3/1x,'Su=',e10.3/1x,'Fa=',
     $e10.3///' hit enter to continue')
      read(*,*)

      WRITE(*,150)
  150 FORMAT(' Time (sec)',T25,'Fa',T45,'Fr',T60,'epsX')

      DO 1000 tmax=0,10000000

       tlapse= 1. + tmax*DN

       CALL CREEP(tlapse,MATPRO,PRNSTR,nomatl,noang,N,M,DT,crpstr)

       CALL CLT(nomatl,noang,N,M,DT,PRNSTR,crpstr)
```

```
C     READ(*,*)
      SA2= PRNSTR(1,1)

      BIGN2= 10**(((SA2/SU-A)/B)**(1./P))

      TAU2= (tlapse+DN)/( BIGN2 )

      DTAU= (TAU2-TAU1)/DN

      FA2= SA2/SU

     INTGRL= INTGRL + ( (1-FA1)*Jvar*(TAU1)**(Jvar-1.)*DTAU +
    $      (1-FA2)*Jvar*(TAU2)**(Jvar-1.)*DTAU )/2.D0 * DN

     FR= 1.D0 - INTGRL
     WRITE(*,200) tlapse, FA2, FR, crpstr
     WRITE(6,210) tlapse, FA2, FR, crpstr
 200 FORMAT(T1,E10.3,T20,F7.4,t40,F7.4,t55,e10.3)
 210 FORMAT(1X,E10.3,1X,F7.4,1X,F7.4,E10.3)
     IF(FR .LE. FA2) stop

     SA1= SA2
     BIGN1= BIGN2
     TAU1= TAU2
     FA1= FA2

1000 CONTINUE

     STOP
     END


C  ************** subroutine CREEP  ******************************

      SUBROUTINE CREEP(tlapse,MATPRO,PRNSTR,nomatl,noang,N,M,DT,crpstr)

     INTEGER nomatl,noang
     DOUBLE PRECISION N(3), M(3), DT, MATPRO(10,12), PRNSTR(3,151),
    $              crpstr
     REAL S11o, A1, b1,
    $     S22o, A2, b2,
    $     S66o, g, p, f, q,
    $     tlapse, E1, E2, G12, tau12,tau122



C  These constants define the creep in the 0-degree direction:

     S11o= 2.07e-11
       A1= 2.97e-13
       b1= 0.2
```

```
      E1=1./(S11o + A1*(tlapse)**b1)
       MATPRO(1,1)= E1
       MATPRO(2,1)= E1
       MATPRO(3,1)= E1

C  These constants define the creep in the 90-degree direction:

     S22o= 5.62e-11
       A2= 3.629e-13
       b2= 0.355

       E2= 1./(S22o + A2*(tlapse)**b2)
       MATPRO(2,2)= E2
       MATPRO(1,2)= E2
       MATPRO(3,2)= E2


C  These constants define the shear creep response:

     S66o= 1.1e-10
       g= 1.0e-16
       p= 2.77e-15
       f= 2.23e-14
       q= 0.37

C  It is necessary to cycle G12 and tau12 calculations until there
C  is convergence:

  100   tau12= PRNSTR(3,3)
      tau122= tau12*tau12
       G12= 1./( S66o*(1.+g*tau122) + p*(1+f*tau122)*tlapse**q )
       MATPRO(3,3)= G12
       CALL CLT(nomatl,noang,N,M,DT,PRNSTR,crpstr)

       IF(ABS(tau12-PRNSTR(3,3)) .LT. ABS(0.01*tau12)) RETURN

       GOTO 100


      RETURN
      END

C  ********** subroutine data ******************************

      SUBROUTINE DATA(plies,nomatl,angles,noang,matpro,name,stack,
     $                N,M,DT)

C  variable definitions
C    N(i), M(i)  [dbl]   the force and moment resultants
C    plies       [int]   The number of lamina in the laminate
```

```
C    nomatl      [int]   The number of different lamina materials.
C    matpro(,)   [dbl]   E1, E2, G12, Nu12, thickness, cte1, cte2,
C                        Xt,Xc,Yt,Yc,S
C    name()      [chr]   material names (40 characters max.)
C    stack(,)    [int]   Stacking sequence: matl. #, angle
C    angles()    [int]   the different ply angles expected
C    noang       [int]   the number of different angles to read
C
C  example data file (all unformatted):
C
C  4             this tells the number of angles.
C  0,90,45,-45   there are four angles: 0, 90, 45 and -45.
C  4, 2          four plies, and two materials used, integer
C  30.0e6,.75e6,.37e6,.3,.005,-1e-7,13e-6 E1,E2,G12,Nu12,thick,cte1,cte2
C  110e3,75e3,5e3,13e3,20e3              Xt,Xc,Yt,Yc,S;
C  ..... as many doublerows as matls. used.
C  'T300/5208 graphite/epoxy'
C  'P75/ERL-1962 graphite/epoxy'
C  1,   0        <--
C  2,  90         |---- the stacking sequence consists of
C  1,  45         |     the material #, followed by the ply angle.
C  1, -45 etc.   <--
C  -82.5         difference between the use and cure temp.
C  1E6,0,0,0,0,0  the force and moment resultants


      character*40 name(10)
      integer i,j,plies,nomatl,stack(150,2),angles(50),noang
      double precision matpro(10,12), N(3), M(3), DT
      open(unit=3,file='LIFE.DAT')

      read(3,*) noang
      read(3,*) (angles(i), i=1,noang)
      read(3,*) plies,nomatl
      read(3,*) ((matpro(i,j), j=1,12), i=1,nomatl)
      read(3,*) (name(i), i=1,nomatl)
      read(3,*) ((stack(i,j), j=1,2), i=1,plies)
      read(3,*) DT
      read(3,*) N(1),N(2),N(3),M(1),M(2),M(3)
  700 continue

      return
      end
```

Vita

J. André Lavoie was born in Salem, Massachusetts on July 21, 1962. He did not stay there, but promptly moved to Alaska, courtesy, U.S. Army. After a lengthy 32 months, split between Anchorage and Fairbanks, he moved back to Salem to wait the 12 months for his Dad to return from Viet Nam so he could learn to tie his shoes. Out of necessity, he learned to tie them himself. He credits this early experience in experimental mechanics with setting the stage for an adult career in engineering.

He gained his B.S. degree in Engineering Science and Mechanics from Virginia Polytechnic Institute in 1986, which included one year of Cooperative Education work experience at the Naval Research Lab in Washington D.C. While there, he was involved with fatigue and creep testing of gas turbine engine materials. His Senior project was on computed aided alignment of hydraulic tensile test machines. He eventually found a job with Lockheed Engineering and Sciences Company at NASA Langley Research Center where he worked as a composite materials test engineer for nearly four years. The highlight was involvement in a project to build an IR interferometer test facility for measuring thermal distortion of composite mirrors in a simulated space environment. After much delay, he published the results of his Senior Project in Experimental Techniques and won a 1990 Best Technical Paper Award from the Society for Experimental Mechanics.

By Spring of 1991, he was preparing himself for graduate school. To do so properly, he would need to become as destitute as the other students who were continuing on directly from undergrad. A six month trip around the globe was planned to the hot places of the world. Included on the itinerary were the beautiful islands of Hawaii, New Zealand, Bali, and Koh Pee Pee, Thailand. Time was well spent in big countries like Australia (home of termite mounds, crocodile pies, and Kangaroo curry). India had much better food, whether it was in the states of West Bengal, Uttar Pradesh, or Rajahstan. From Bombay, it was off to Kenya for four wheel driving in Turkana, and to do big game spotting in the Masai Mara. By the time he had returned home to Virginia, he had increased his tally of countries visited to over twenty-five.

A Master of Engineering degree was taken at V.P.I. His project was on the design of a new test method for crush energy absorption of composite plates. He (and his two co-authors) won a Prize for Most Outstanding Paper published in 1995, in the Proceedings of the Institution of Mechanical Engineers, in the area of materials and solid mechanics. He continued study for the Ph.D., which brought with it special opportunities to perform part of his research at the Defence Research Agency in England, visit other research centers in Sweden and Italy, and present some of his work at conferences in Italy, and Portugal. André has no idea where life will take him next, but it will not be alone. He met his then future wife, Chiara from Italy, at Virginia Tech International Club's regularly held Friday coffee hour in the Cranwell International Student Center.

J. André Lavoie